



DIPLOMARBEIT

Development of a LA-ICP-MS procedure for stoichiometry analysis of ternary boride thin films

unter der Anleitung von

Associate Prof. Dipl.-Ing. Dr. techn. Andreas Limbeck
Univ. Ass. Dipl.-Ing. Dr. techn. Helmut Riedl

ausgeführt am

Institut für Chemische Technologien und Analytik
Technischen Universität Wien

durch

Maximilian Weiss BSc
Matrikelnummer 01326639
Neugasse 13
7471 Rechnitz

Wien, 1. Oktober 2018

Maximilian Weiss, BSc.

Acknowledgments

First, I would like to express the deepest appreciation to my supervisor Andreas Limbeck, for giving me the opportunity to be part of his working group. He always had an open ear for my concerns and provided me advice and practical suggestion without this thesis would not have been possible. I want to thank Helmut Riedl for providing the collaboration which enabled me to work on this interesting topic. My colleges in the group provided a great working climate and made the last six months a pleasurable time. Especially I want to thank Lukas Brunnbauer and Christopher Herzig for their practical support in everyday lab live. The completion of my studies would not have been possible without the support and encouragement I got from my family and friends, for which I am extremely grateful.

Abstract

Borides of the transition metals are a relatively new class of hard materials, which show hardness combined with ductility, chemical resistance and good wear behavior. These properties are known to depend on the composition, especially the number of boron vacancies plays an important role, also the addition of alloying metals can be used to improve the material behavior. In this thesis analytical procedure for stoichiometry determination of ternary borides based on tungsten diboride alloyed with aluminum, tantalum and vanadium was developed. The ternary thin films were prepared using Physical Vapor Deposition (PVD). To overcome the limitations of X-Ray based methods usually applied for thin film analysis, a Laser Ablation Inductively Coupled Plasma Mass Spectrometry (LA-ICP-MS) method was developed to determine the stoichiometric composition of the thin films. As a relative method LA-ICP-MS requires the use of standards, which have to match the matrix, to quantify the signals. Availability of such standard materials is limited, especially for the innovative and new compound class of ternary borides. For this, a new calibration approach so called microgrooves was used. These are trenches in a substrate material which are produced by laser ablation. These grooves are filled with a liquid standard, which would be easily prepared by mixing respective element standard solutions, thereby the composition of the standards could be adjusted to the need of the experiment. This combines the advantages of a direct solid sampling method such as no sample preparation, little sample consumption and the ability of spatially resolved measurements with ease of use of liquid standards. For comparison the thin films were dissolved and measured by liquid ICP-OES, which showed a good agreement of the data, but was time consuming and involved the use of hazardous chemicals. Further the use of LIBS for the measurement of the thin films was tried. It was shown that quantitative measurements are possible, however the microgroove standards could not be used due to the higher levels of detection of this method.

Kurzzusammenfassung

Die Boride der Übergangsmetalle sind eine relativ neue Klasse der Hartstoffe, die sich durch ihre überragenden Eigenschaften, wie Härte kombiniert mit Duktilität, chemischer Beständigkeit und gutem tribologischen Verhalten, auszeichnet. Es ist bekannt, dass diese Eigenschaften stark von der Zusammensetzung des Materials abhängen, insbesondere der Konzentration an Bor Leerstellen und sich durch die Zugabe von Legierungselementen verbessern lässt. In dieser Arbeit wurden ternäre Boride untersucht die auf Wolframbiborid basieren, welches mit Aluminium, Tantal oder Vanadium legiert wurde und mittels physikalischer Gasphasenabscheidung (PVD) als dünne Schicht abgeschieden wurde. Um die Limitierungen der für die Dünnschichtanalyse häufig eingesetzten Röntgenmethoden zu überwinden, wurde eine auf Laser-Ablation Induktiv-gekoppelter Plasma Massenspektrometrie (LA-ICP-MS) basierende Methode zur Bestimmung der Stöchiometrie dieser Proben entwickelt. LA-ICP-MS benötigt als relative analytische Methode Standards, die die Eigenschaften der Probenmatrix widerspiegeln sollten, um die erhaltenen Signale zu quantifizieren. Solche Materialien sind jedoch oft nicht verfügbar, besonders für eine neue Materialklasse wie die Boride. Dazu wurde ein neues Kalibrationsverfahren verwendet, sogenannte 'Microgrooves'. Dabei handelt es sich um Furchen, die mit Laser -Ablation hergestellt werden und in die eine flüssige Standardlösung eingebracht wird. Mit diesem Verfahren lassen sich die Vorteile einer direkten Feststoffmessung, wie die geringe Probenvorbereitung, die fast zerstörungsfreie Messung sowie die Möglichkeit, Daten ortaufgelöst zu gewinnen, mit der Einfachheit der Herstellung von flüssigen Standardlösungen kombinieren. Flüssigstandards lassen sich einfach durch das Mischen von Einzelelementstandards herstellen und sich so auf die Bedürfnisse des Experiments anpassen. Zum Vergleich wurden die Proben aufgeschlossen und mit ICP-OES gemessen, was eine gute Übereinstimmung der Ergebnisse ergab. Flüssigmessungen sind aber vergleichsweise zeitaufwändig. Zusätzlich wurde der Einsatz von LIBS zur Messung der dünnen Schichten erprobt. Es konnte gezeigt werden, dass die quantitative Messung prinzipiell möglich ist, der Einsatz der Microgroove Standards aufgrund der höheren Nachweißgrenzen jedoch nicht.

Contents

1	Introduction	1
2	Theory	3
2.1	Preparation of thin films	3
2.1.1	Boride thin films	3
2.1.2	Preparation of thin films with PVD	3
2.2	Analysis of thin films - Liquid measurements with ICP-OES	5
	Principles of liquid ICP-OES	5
	Instrumentation of ICP-OES	6
2.3	Analysis of thin films - direct solid sampling	6
2.3.1	LA-ICP-MS	6
	ICP-MS	6
	Plasma	7
	Sample introduction	8
	Vacuum interface and ion optics	8
	Mass analyzers	8
	Interferences	10
	Detectors	10
	Laser Ablation	10
	Principles	10
	Instrumentation	11
	Quantification strategies	11
2.3.2	LIBS	12
	Principles	12
	Instrumentation and data treatment	13
2.3.3	ERDA	14
3	Experimental	15
3.1	Chemicals	15
3.2	Sample fabrication	15
3.3	Bulk measurements using liquid analysis	18
3.3.1	ICP-OES	18
3.3.2	Sample digestion	18
3.4	Bulk measurements using direct solid sampling	19
3.4.1	LA-ICP-MS	19
3.4.2	LIBS	20
3.4.3	Surface profiles and SEM measurements	21
3.4.4	Quantification strategy	21

3.4.5	Fabrication of microgrooves	22
4	Results and Discussion	24
4.1	Liquid analysis	24
4.2	Microgroove calibration	24
4.2.1	Choice of material and preparation	24
4.2.2	Optimization of LA-ICP-MS analysis	25
4.2.3	Microgroove calibration	28
4.3	Comparison of results	29
4.3.1	AlWB, WB and AlB samples	30
4.3.2	VWB samples	32
4.3.3	TaWB samples	34
4.4	Whole wafer measurements	35
4.5	LIBS	35
4.5.1	Optimization of parameters	35
4.5.2	Calibration through line ratios	35
5	Conclusion and Outlook	41
A	Appendix	43
B	List of abbreviations	51

1 Introduction

Hard protective coatings are widely used on tools and engineering parts to improve the wear and corrosion resistance. Traditional materials include nitrides and carbides. Borides of the transition metals are a rather new class of hard materials. Their favorable properties include hardness combined with ductility as well as chemical resistance and good wear behavior. To deposit these materials physical vapor deposition (PVD) techniques, like sputter coating, are used, because chemical vapor deposition (CVD) techniques with boron containing gases are difficult to employ.[1] The properties of these materials depend on the micro structure and the composition. In [2] it was shown that the number of boron vacancies influences the hardness of TiWB_2 thin films. It is known that elemental fractionation effects can occur during sputter deposition, so that the composition of deposited material can differ from that of the target material.[3] Further PVD deposition favors the formation of vacancies in materials.[4] For this reason it is important to have a method for the determination of the stoichiometric ratios in thin films. Because of the low number of electrons, boron is hard to measure with the popular X-Ray based methods like X-Ray diffraction (XRD) and X-Ray fluorescence. Measurements of the composition of boride thin films have been reported in literature using several methods. In [5], depth profiles of tantalum diboride films were recorded using secondary ion mass spectrometry (SIMS), in [6] the metal to boron ratio of TaB_2 and HfB_2 films deposited by magnetron sputtering was measured using SIMS and Auger electron spectroscopy (AES) and electron probe microanalysis (EPMA), employing a one point calibration with a HfB_2 sample of known composition. Jiang et al. [7] used X-Ray photo-electron spectroscopy (XPS) to determine the composition of WB_2 coatings. In [2], TiWB_2 layers were digested and measured with liquid ICP-OES. Another method which is especially suitable for light elements is elastic recoil detection analysis (ERDA) which was used in [8] for $\text{Ta}_{1-x}\text{W}_x\text{B}_2$ films, which is reported to have an accuracy of 1 at% for boron, but has difficulties to distinguish tantalum and tungsten. Some of the samples used in this thesis were also measured with this method and the values were used for comparison. Because the aforementioned methods involve a rather low sample throughput and require the use of sophisticated equipment, an improved and more simple procedure would be desirable.

This thesis focuses primarily on the use of laser ablation inductively coupled plasma mass spectrometry (LA-ICP-MS). LA-ICP-MS is a direct solid sampling technique, which removes material from the sample with a laser beam and determines the elemental composition with an ICP-MS instrument. It has the advantage that it needs little sample preparation, has a low sample consumption and enables spatially resolved measurements of most elements in the periodic system. LA-ICP-MS is a relative analytical method and requires standard materials to infer from the signals to the amount of analytes.

These standards need to resemble the properties of the samples as closely as possible because of matrix effects during the laser ablation. [9] In a prior paper of the working

group [10] the composition of Mo-Si-B films was determined by LA-ICP-MS using multi variant calibration. Samples were digested, the stoichiometry was determined by liquid ICP-OES and these values were used to build a multi linear model for the LA-ICP-MS. A disadvantage of this approach is the need for the rather laborious dissolution process, which involves the use of dangerous chemicals, in this case hydrofluoric acid.

A further advantage is the possibility of spatially resolved measurements, which enables to access the homogeneity of the films and the measurements of whole wafers. A simpler approach would be to use dried droplet standards for laser ablation. Nischkauer et al. [11] used the approach of microgrooves for the determination of lead in blood. The idea behind microgrooves is to prepare liquid standards, which is rather easy, pipette them in the microgrooves, which are small cavities of fixed size, let the liquid dry and measure the cavities with the ablation apparatus. This method seems suitable for the question in this thesis, because the interest lies in the element ratios and not in the absolute concentration, the absolute quantity of analyte in the microgroove does not need to be known.

The approach in this thesis was the following: ternary boride thin films based on tungsten diboride alloyed with tantalum, aluminum or vanadium deposited by PVD were supplied in a cooperation by Helmut Riedl . Of each sample a part was digested and measured by ICP-OES. These values were considered as reference values for the overall composition because liquid ICP-OES is a well established and trusted method with relative errors in the range of about 1 %. For the LA-ICP-MS measurements microgrooves with liquid standards were used for calibration. The same calibration approach was employed with LIBS (Laser Induced Breakdown Spectroscopy), another promising analytic technique.

2 Theory

2.1 Preparation of thin films

2.1.1 Boride thin films

Thin films are used in industry to improve the properties of surfaces in respect to hardness, wear and corrosion resistance. A class of materials which fulfills these requirements are metal borides. [12] Diborides of the transition metals tend to crystallize the hexagonal so called AlB_2 structure with the space group 191 (P6/mmm) or the so called W_2B_5 structure with the space group 194 (P63/mmc). (Figure 2.1) [8] The AlB_2 structure is metastable for pure WB_2 [13], but can be stabilized through point defects and the addition of alloying metals [8]. The AlB_2 structure consists of graphite like honeycomb boron layers and metal layers, with metal ion placed above the center of the honeycombs. In the ternary borides the metals form ideal solid solutions on the metal sites. An important property is their ability to form boron vacancies [14], so their stoichiometry generally is AB_{2-x} .

2.1.2 Preparation of thin films with PVD

The thin film samples used in this thesis were prepared with sputter coating, which is a PVD technique. Sputter coating is a physical vapor deposition method for the production of thin films. In this technique, atoms are ejected from a target via a bombardment with particles. The ejected material then deposits on the substrate. A schematic of a basic sputtering apparatus can be seen in Figure 2.3 Sputtering is carried out under vacuum conditions, with inert residual atmosphere or in a low-pressure reactive atmosphere to produce e.g. oxides or nitrides when sputtering under oxygen or nitrogen gas. The material deposited on the substrate can differ in the composition from the target, possible reasons can be that one element gets ejected preferably from the target or that, especially light elements get lost on their way through the gas phase to the substrate. The bombarding particles are often ions from a low-pressure plasma, usually argon, because of its high atomic weight, are used which are accelerated towards the surface through a electric field, which can be applied as DC (direct current), AC (alternating current) and HF (high frequency). In magnetron sputtering, a magnetic field confines the plasma electrons near the surface of the target and can bend them to closed paths, which increases the density of the plasma. When multiple anodes of different materials are used alloys in arbitrary composition can be produced. The sputtering targets are typically cooled, the substrates are heated for an optimized film growth. In a sputtering apparatus target or substrates are moved to ensure a even deposition of the film. [3]

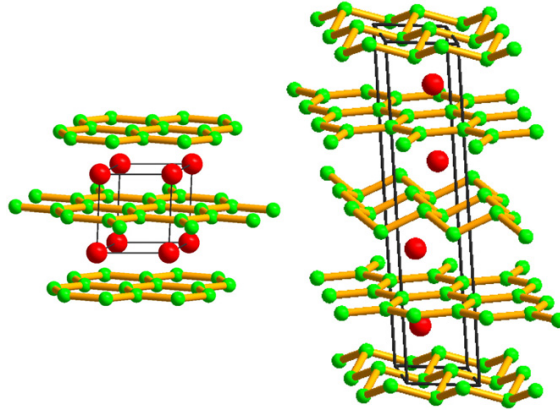


Figure 2.1: Crystal structure of WB_2 in the 191 space group (left) and the 194 space group, from [12].

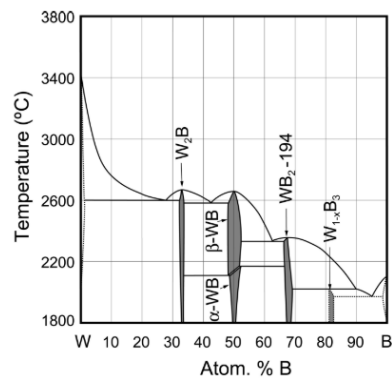


Figure 2.2: Phase diagram of the W-B system from [14], note that WB_2 in space group 191 is metastable and doesn't appear in a equilibrium phase diagram.

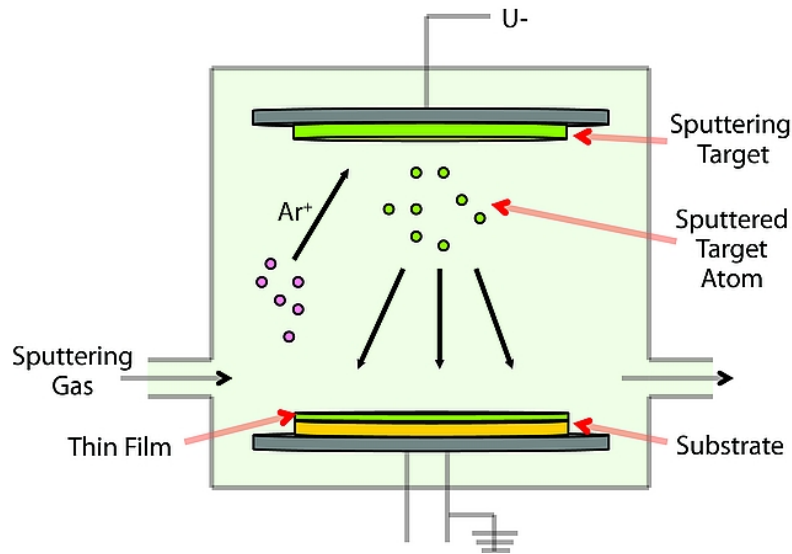


Figure 2.3: Schematics of a simple sputter coating apparatus, from [15].

2.2 Analysis of thin films - Liquid measurements with ICP-OES

Principles of liquid ICP-OES

Inductively coupled plasma optical emission spectroscopy is an analytical technique for quantitative elemental characterization based on the emission of characteristic elemental lines from an inductively coupled plasma. It has the ability to measure most elements of the periodic system simultaneously, has limits of detection in the $\mu\text{g/L}$ range and a high dynamic range. The plasma is formed the same way as in 2.3.1. The temperatures in the plasma are high enough to excite electronic states of atoms and ions, which emit light during their relaxation. Beside elemental lines, also ionic lines of the elements can be observed, due to the ionization of some elements in the plasma. The degree of ionization depends on the temperature of the plasma, which depends on the viewing height. The viewing height of the measurement is therefore an important consideration. Molecules which are formed mainly at lower temperatures can emit continuous radiation, which yields a background signal to the measurements. For liquid measurements the sample has to be brought into solution. This is achieved for most solid samples by acid digestion. For the boride thin films on silicon wafers used in this thesis, a combination of concentrated nitric and hydrofluoric acid is used. The nitric acid is a strong acid and oxidation agent, the hydrofluoric acid is needed to bring the silicon substrate into solution and to stabilize the transition metals in solution as fluoro complexes. The use of liquid samples has the advantage that it is rather simple to prepare external standards, but has the disadvantage that it is time consuming, a large portion of the sample is needed and that spatial information is lost during the dissolution.

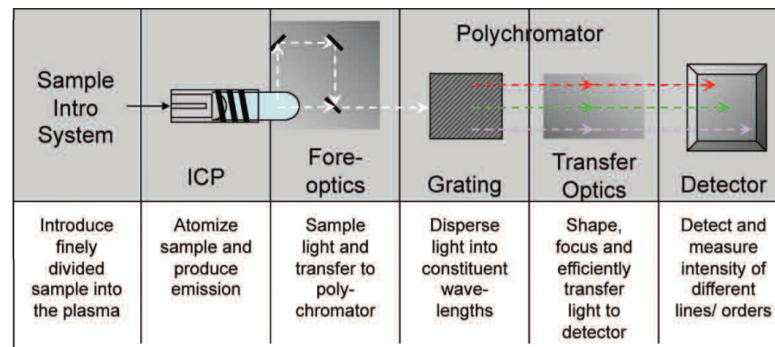


Figure 2.4: Schematics of the components of a ICP-OES system[17].

Instrumentation of ICP-OES

An ICP-OES instrument consists of the sample introduction system, the plasma torch and the spectrometer system (Figure 2.4). The sample introduction and plasma formation is analogous to ICP-MS, as described in 2.3.1. There are two configurations available: axial and radial (see Figure 2.5). In axial mode the lines are monitored from the front in the radial mode by the side. The axial mode has lower detection limits, because of the longer optical path, but is less robust and has a higher background signal, because colder regions with more molecular emission are also observed. The spectrometer consists of dispersive elements, which separates the wavelengths, and a detector. The lines of some elements lie in the deep UV region, where the optical absorption of air becomes significant, therefore the optical system has to be kept under vacuum or argon atmosphere. As dispersive elements optical gratings are used. Common types are Czerny-Turner and Paschen-Runge geometry. Another common type are Echelle spectrometers, which have two dispersive elements, a grating and a prism. Photomultiplier tubes (PMT) and solid state detectors such as CCD (charged coupled device) and CID (charge injection device) are used as detectors. Photomultiplier tubes offer the highest sensitivity, but are limited to the observation of a single wavelength. With CCD and CID it is possible to cover the whole spectrum and measure all elements simultaneously. In combination with Echelle monochromator two dimensional detectors are used, where each line captures a different order of diffraction. CID detectors are not prone to blooming effects, which means that if a pixel gets saturated, the charge spreads to neighboring pixels, and makes it hard to measure weak lines in the neighborhood of strong ones. [16]

2.3 Analysis of thin films - direct solid sampling

2.3.1 LA-ICP-MS

ICP-MS

Inductively Coupled Plasma Mass Spectrometry (ICP-MS) is a method for elemental analysis based on the ionization of the sample in a plasma and the separation of the

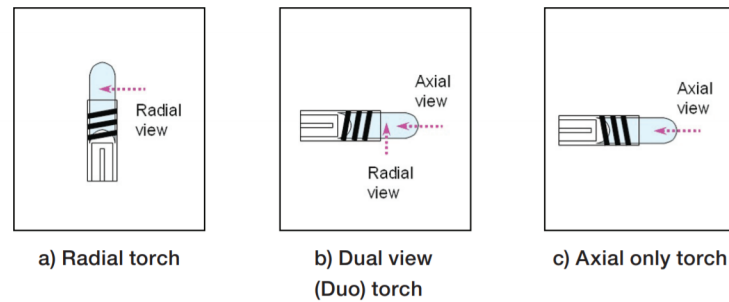


Figure 2.5: In ICP-OES the emitted light can be viewed radial to the torch (a), axial to the torch (C) or both axial and radial (b) [17].

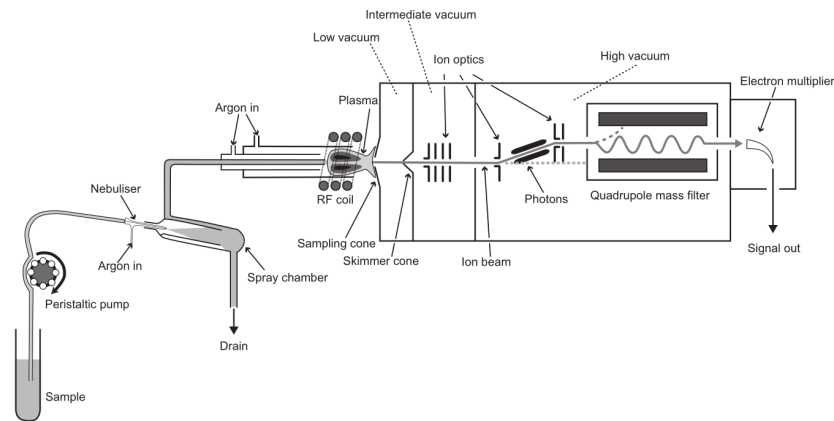


Figure 2.6: Schematics of a simple Quadrupole ICP-MS, from [18].

generated ions in a mass spectrometer. Nowadays ICP-MS is a very powerful tool for trace element analysis down to sub ppt (parts per trillion) concentrations while offering up to nine orders of magnitude of dynamic range. The components of a ICP-MS instrument are described in detail in the following sections. A schematics of the device is given in Figure 2.6. [18]

Plasma

Almost all ICP instruments operate with an argon plasma. The plasma is primarily ignited with a spark. A RF electric field with a frequency of either 27 or 40 MHz is applied through a coil. It is generated with a RF generator with a power in the range of 1000 W to 1500 W. The plasma torch consists of three concentric tubes, usually made of fused silica or ceramic. The sample gas flow is injected through the inner tube, a auxiliary argon gas flow in the middle tube and a cooling gas flow, which is the highest through the outer tube. The last one shield the torch from the plasma and prevents it from melting and also shapes the plasma cone. The plasma has a temperature of several thousand

kelvin. The sample is desolvated, atomized and finally ionized. The ionization occurs mainly due to the collision of the atoms with argon ions, which have an ionization energy of 15.2 eV, which is enough to ionize most elements in the periodic system, except helium, neon and fluorine. [18] After then ions are forced to curved paths through an alternating HF electromagnetic field.

Sample introduction

There are different possibilities to introduce samples into the plasma. Liquid samples are dispersed to a aerosol of micrometer sized droplets with the assistance of a nebulizer. Nebulizers are most often operated pneumatically, where the liquid flows into the argon gas stream. A spray chamber behind the nebulizer hinders too large droplets from entering into the plasma. The reason for this is that they couldn't be evaporated completely in the plasma. The separation of the droplets is based on the higher inertia of larger droplets, which cannot follow the gas flow and get deposited on the wall of the spray chamber. Common types are the cyclonic spray chamber and the double pass spray chamber. A drawback of the spray chamber that only about 2 to 5 % of the sample reaches the plasma. Direct solid sampling methods include laser ablation, see Section 2.3.1 and ETV (electro thermal vaporization), where a sample is heated in a graphite furnace in presence of certain additives to create a gas or aerosol, which is carried by a gas flow into the plasma. [16]

Vacuum interface and ion optics

The generated ions have to be transferred from the plasma, which has atmospheric pressure, into the high vacuum section of the mass analyzer. This is accomplished by a two staged interface consisting of a sampler and a skimmer cone with an intermediate vacuum between them. The cones are typically made of nickel and have a millimeter sized orifice. The vacuum inside the device is maintained by turbomolecular pumps which are backed by rotary vane pumps. The ions are focused by electrostatic lenses and guided to the mass analyzer section. [18][19]

Mass analyzers

The mass analyzer separates charged species based on their mass to charge ratio (m/z). In ICP-MS quadrupole, time of flight and sector field are the most common. In sector field mass analyzer the ions are separated by the Lorenz force in a magnetic field:

$$F = q(E + v \times B) \quad (2.1)$$

The ions are forced to curved paths with a radius depending on the m/z ratio.

$$\frac{m}{z} = \frac{B^2 * r^2 * e}{2 * V} \quad (2.2)$$

By varying the magnetic field strength, different ions are allowed to pass to the detector. Because the ions leaving the plasma have a certain distribution of their kinetic energy,

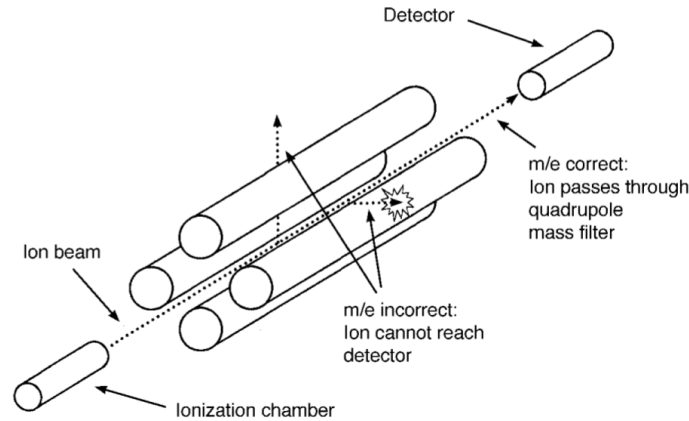


Figure 2.7: Schematics of a quadrupole mass analyzer, from [20].

which would limit the resolution, in a so called double focusing instrument an electrostatic analyzer is placed after the magnetic. The sector field instrument has the highest resolution, up to 12000, but has a high cost and a low scan speed.

In time of flight instruments ions are injected as packages into a flight tube of certain length. Their m/z determines the amount of time they need to reach the detector:

$$F = 2qU\left(\frac{t}{L}\right)^2 \quad (2.3)$$

Time of flight analyzers are the fastest and have a rather high resolution, but have the drawback that a reasonable use requires pulsed sources, e.g. laser ablation, while otherwise big parts of ions, that are generated during the TOF cycles would be lost, which would mean a loss of sensitivity.

A quadrupole mass analyzer consists of four rods, arranged parallel to the ion path. Between the rods a static and an oscillating voltage is applied:

$$\phi = U - V * \cos(2\pi * f(t - t_0)) \quad (2.4)$$

The motion of the ions in this field is governed by the so-called Mathieu equations. With U and V fixed, only a certain m/z ratio has a stable trajectory through the mass analyzer. By varying U the m/z is scanned across the elements of interest. The quadrupole mass analyzer is the cheapest and the most commonly used. It can scan through the mass range rather quickly but has the drawback of a low resolution of about 1, which does not allow to separate interferences. Therefore, it is usually combined with a collision/reaction cell, see next section. The time the quadrupole stays on a certain mass is called dwell time, the time it needs to change to another is called settling time.

[18][19]

Interferences

A problem in ICP-MS analysis are interferences. This means that there exist a species with a mass to charge ratio which cannot be separated from the element of interest due to an insufficient resolution of the mass analyzer, which is defined:

$$R = \frac{m}{\Delta m} \quad (2.5)$$

Interferences can occur due to isobaric species, like $^{40}\text{Ar}^+$ for $^{40}\text{Ca}^+$, polyatomic ions, like $^{14}\text{N}_2^+$ for $^{28}\text{Si}^+$ or multiple charged species, like $^{28}\text{Si}^{2+}$ for $^{56}\text{Fe}^{2+}$. Strategies for reducing such interferences include careful choice of the matrix and the plasma conditions, employment of collision/reaction cells and the use of high-resolution mass analyzers. In a collision/reaction cell gas is introduced at low pressure. In the kinetic energy discrimination (KED) mode, an inert gas is introduced in the cell. Polyatomic species have a larger collision cross-section than single ions. Though collisions they lose kinetic energy and can be prevented by a potential from entering the mass analyzer. In a reaction cell the gas selectively forms a chemical compound with some ions, which has a different m/z ratio and can therefore be separated by the mass analyzer.

Detectors

The detector converts the ion current into pulses which are counted. In ICP-MS electron multipliers and Faraday cups are used. In electron multipliers, which exist in the form of discrete or as continuous dynode, the impacting ion releases electrons from a surface, which are accelerated and again hit a surface so that more electrons are released and the pulse is intensified. A Faraday cup is simply a electrode that collects the ions . A cage is build around the electrode, which prevents the secondary electrons from escaping the detector. For a high dynamic range, simultaneous mode detectors are used. These consist of a discrete dynode electron multiplier. For high ion counts, only the first amplification stages are used, and the electrons is collected by a Faraday cup as an analog signal. For low ion counts all amplifying stages are used and the signal is collected as pulse count. [19] [18]

Laser Ablation

Principles

Laser ablation is a direct solid sampling technology with wide applications in analytical chemistry. The idea is that a laser beam removes sample material from a surface, which can then be analyzed by a hyphenated instrument. Advantages of the method is that sample preparation steps like dissolution can be avoided, so that "high tech materials", which are hard to bring into liquid phase, like oxides, carbides, nitrides and borides, are analyzable. It also enables spatially resolved measurements. The mechanism of laser ablation involves the absorption of the laser light, heating and evaporation of the sample. A certain threshold fluence of the laser radiation is necessary to induce ablation. The ablated material forms an aerosol which is carried away by a gas stream. Typically, pulsed lasers

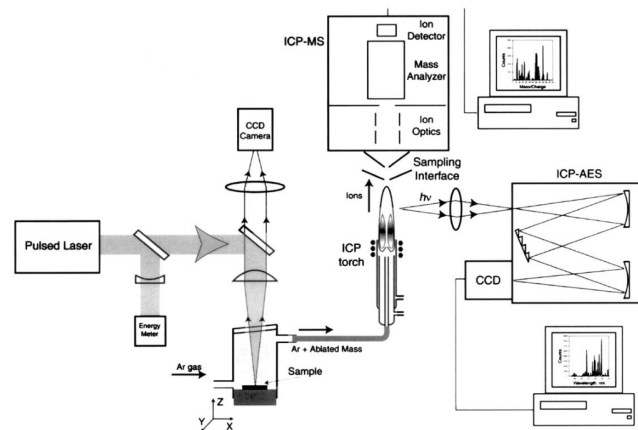


Figure 2.8: Schematics of a laser ablation apparatus, couples to a ICP-MS/OES, from [21].

are used with pulse length from the nano- to the femtosecond range. Femtosecond lasers are reported to give better results due to a smaller sized aerosol and more even shaped craters, which stems from less heat dissipation in the sample. In nanosecond ablation, the ablation onsets during the pulse which yields an effect called plasma shielding, so that a significant amount of the laser energy is not transferred to the sample. A drawback of femtosecond ablation is the much higher price of the instrument. [21] [22] [23]

Instrumentation

A laser ablation apparatus basically consists of the laser, the sample stage in the ablation chamber and the transport tubing, a schematic is shown in Figure 2.8. Different kind of lasers have been used, including Nd:YAG, ruby, CO₂, Ti:Sapphire and excimer lasers. Properties of the laser which are influential are its wavelength, pulse energy and pulse length. Wavelength from the infrared down to the deep UV have been used, where shorter wavelengths lasers give a higher ablation efficiency and less fractionation.[21] Therefore Nd:YAG lasers, which have a fundamental wavelength of 1066 nm are frequency multiplied to 266 nm or 213 nm. In Nd:YAG lasers, the active medium is a single crystal garnet doped with Neodymium ions. Pulsing of the laser is achieved via Q-switching. The sample is placed on a movable stage and is monitored with a integrated microscope which allows the selection of the ablation region. The ablation is performed under noble gas atmosphere, with helium giving the best results. The gas flow transports the generated aerosol into the plasma of the ICP-MS. [21]

Quantification strategies

To relate the signal of an analytical device to the concentration in the sample, it is necessary to calibrate the system. A problem in laser ablation measurements are the effects of "elemental fractionation", where the detected signals are not representative of the analyzed sample. Errors due to matrix effects can occur during the ablation, the

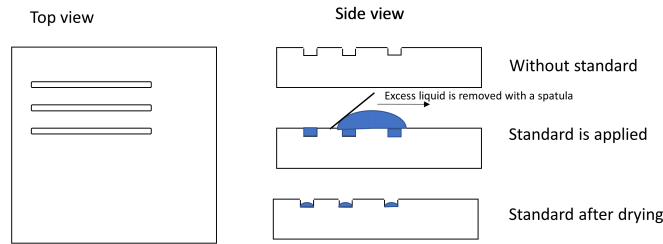


Figure 2.9: Schematics of the microgroove concept, microgrooves are small cavities in a substrate. A drop of the standard solution is placed on top of them, excess liquid is removed with a rubber spatula and the solution is let dried. Afterwards the groove is measured in a line scan with the laser ablation apparatus.

transport of the sample to the plasma and in the instrument itself. Strategies involve the use of certified reference materials (CRM), which are unfortunately only available for a few types of samples or the use of matrix matched standard. The idea is to have a standard of known composition which resembles the properties of the sample as closely as possible. Different attempts like pressing powders, addition of standard solution to powders or fusing the sample to borate discs are reported in literature. The drawback of these methods are the significant effort in the preparation these standards, which limits the sample throughput. Internal standards can be applied to correct differences between samples or drifts over time of the apparatus. Another approach is liquid ablation, where liquid standards, which are easy to prepare are used. One approach is the use of dried droplets, in which liquid is placed onto a surface, dried and the residue is ablated by the laser. This simple approach gives rather large spots on the surface, which have to be ablated completely for quantitative measurements. An improvement of this approach is to use of microgrooves. These consist of small cavities, which trap a fixed amount of liquid and can be ablated in a single pass, see Figure 2.9 for a schematic of the concept. [11] [9] [24]

2.3.2 LIBS

Principles

Laser induced breakdown spectroscopy is a prospecting direct solid sampling technique for elemental analyses. The sample is irradiated with a laser beam to ablates material. The ablated material becomes atomized, ionized and forms a plasma. The high temperature of the plasma yields in the excitation of electrons, which emit characteristic elemental lines during their relaxation to the ground state. LIBS has unique analytical capabilities, it is possible to analyze solid, liquid or gaseous samples and detect all elements of the periodic system, including hydrogen, carbon nitrogen and the noble gases. LIBS is a direct solid sampling technique which requires minimal sample pretreatment. It can be used for quantitative and qualitative analysis with detection limits down to the ppm range

depending on the element. However, due to matrix effects some effort is often required to obtain quantitative results with high accuracy. [25] In the first step the laser ablates material as described in Section 2.3.1. If the density of free electrons generated by the ablation, which requires a certain laser irradiance, is high enough, avalanche ionization processes generate a plasma. The plasma expands while emitting light. [22] There are different processes which contribute to the emission spectrum: the characteristic atomic and ionic lines of the elements, which are emitted when excited electronic states relax, and a background continuum, which is caused by bremsstrahlung. As these processes vary over time, it is possible to optimize the background to signal ratio by placing the measurement in an appropriate time frame, which is determined by the so called gate delay, the time between the start of the laser pulse and the beginning of the data collection.

Instrumentation and data treatment

The LIBS system consists of three main parts: The laser, the target and the spectrometer. A schematic is given in Figure 2.10. The choice of the laser is determined by the aspect of wavelength, fluence and pulse duration, where the considerations are the same as in laser ablation in Section 2.3.1. The laser is focused onto the surface of the target. The target can either be in a controlled environment, as in a laboratory system or outside the system as in open path measurements, which are used e.g. to determine the composition of rocks on Mars [26]. The atmosphere around the sample has a significant impact on the plasma formation [27]. For laboratory instruments, helium and argon are the most commonly used gases, where argon typically yields higher intensities. [28] The sample is positioned on a movable stage which allows manipulation in three axes to adjust the focus of the laser beam and locate the region of interest. The emission of the plasma is resolved by wavelength by a monochromator and detected. Czerny-Tuner and Echelle monochromators are typically used. The detection can be done by Photomultiplier tubes, charge coupled device (CCD) detectors or ICCD (intensified CCD). The detector is typically gated, which means the detection is initiated at a certain time after the laser pulse to maximize the signal to noise ratio. The gate width is the duration of the measurement of the detector.

A remaining problem of LIBS is the quantification of the results. The simplest approach is univariate calibration, where a single line intensity or intensity ratio is plotted against the concentration or concentration ratio in a standard series. For good results the standard series should resemble the sample as close as possible. Because of the often not satisfying results, more advanced calibration techniques, such as MLR (Multi-linear Regression), PLS (Partial least squares), ANN (Artificial neural network) and SVM (Support vector machine) regression were used.[29] To improve the quality of the spectral data several preprocessing methods were applied in literature, e.g. baseline correction, denoising [26] and resolution of overlapping peaks. There also exist approaches to calibration free LIBS (CF-LIBS), which often try to use mathematical models of the plasma to conclude the concentration in the sample from the emission spectra [29] [30], although these methods are often of limited accuracy.

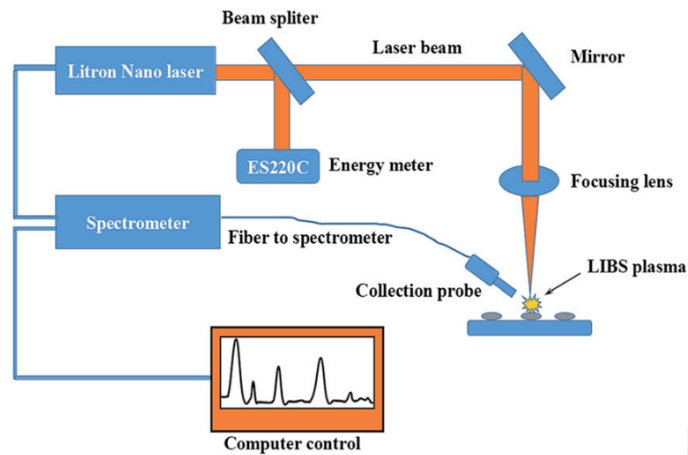


Figure 2.10: Schematics of a LIBS device, from [29].

2.3.3 ERDA

Elastic Recoil detection analysis is a technique based on the scattering between high energy ions (energies in MeV range) and the nuclei of sample. The scattered ions are measured in forward direction. In ERDA the projectile ions must be heavier than the elements in the sample. The composition of the sample and depth profile of the analytes can be calculated from the energy loss of the scattered projectile ions as a function of the scattering angle. ERDA is especially suitable for the measurement of light elements in thin films. It is possible to record depth profiles of surface layers with nanometer resolution. The instrumentation involves a high energy ion accelerator, a vacuum chamber and a energy dispersive ion detector. [31]

3 Experimental

3.1 Chemicals

Ultrapure Water (18.2 M Ω) was prepared with a Barnsted EASYPURE II (Thermo Scientific, USA). Chemicals used are listed in Table 3.1

For ICP-OES measurements, Certipure@ICP standard solutions from Merck (Merck KGaA, Germany) were used.

3.2 Sample fabrication

The thin films were deposited in an in-house built magnetron sputtering system in bottom up configuration equipped with four magnetrons. The procedure was carried out under 0.4 Pa of argon atmosphere and with a measured substrate temperature of 400 °C. 6' Balzers INNOVA design composite targets of the respective binary diborides were used with a target powers up to 11 cm⁻². The sample holder was rotated during the deposition and a bias voltage of 50 V was applied. Further a wafer without rotation of the substrate was fabricated Figure 3.3, where the composition of the thin film varies over the wafer. The phase composition was characterized using X-ray diffraction with a PANalytical XPert Pro MPD diffractometer. These values are listed in Table A.1 in the Appendix. TOF-ERDA measurements were carried out using 36 MeV I⁸⁺ primary ions and a recoil angle of 45 °. [8]

Table 3.1: List of used chemicals.

Name	Formula	Supplier	Quality
Boric acid	HBO ₃	Merck	p.a 99.8%
Sodium Tungstate	Na ₂ WO ₄	unknown	unknown
Tantalum Powder	Ta	Plansee	unknown
Nitric Acid	HNO ₃	Merck	p.a. EMSURE 65%
Hydrofluoric Acid	HF	Merck	p.a. EMSURE 40%
Aluminum nitrate nonahydrate	Al(NO ₃) ₃ *9H ₂ O	unknown	technical
Sodium Hydroxide	NaOH	Merck	p.a 99%
Vanadium(V)oxide	V ₂ O ₅	Acros	98+%

Table 3.2: List of used ICP Standard solutions from Merck

	Catalog Nr	Concentration	Density	Compound
Tungsten	170364	(999 ± 5) mg/kg	1.000 kg/L	$(\text{NH}_3)_2\text{WO}_4$ in H_2O
Tantalum	170356	(1003 ± 5) mg/kg	1.000 kg/L	$(\text{NH}_3)_2\text{TaF}_7$ in H_2O
Vanadium	170366	(987 ± 3) mg/kg	1.013 kg/L	NH_3VO_3 in 2-3% HNO_3
Aluminium	170371	(985 ± 5) mg/kg	1.017 kg/L	AlNO_3 in 2-3% HNO_3
Boron	170307	(1001 ± 3) mg/kg	1.000 kg/L	H_3BO_3 in H_2O

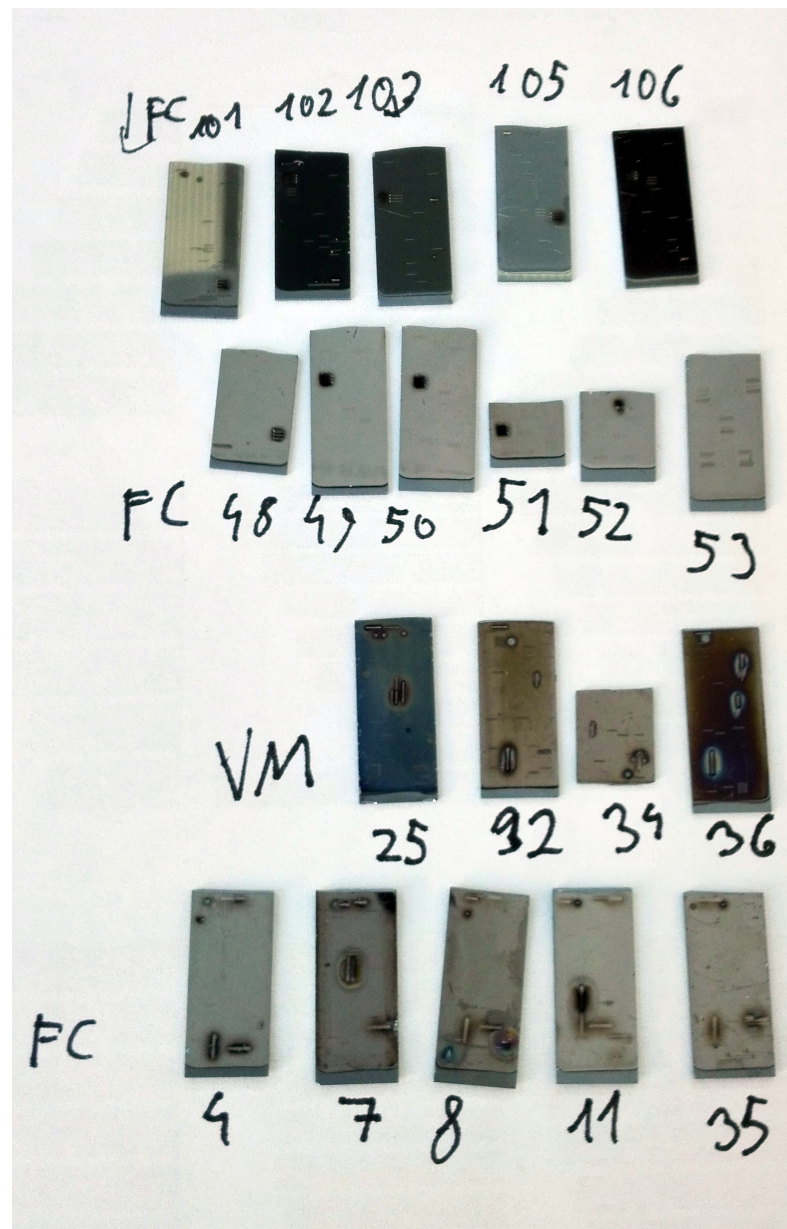


Figure 3.1: Image of the used samples.

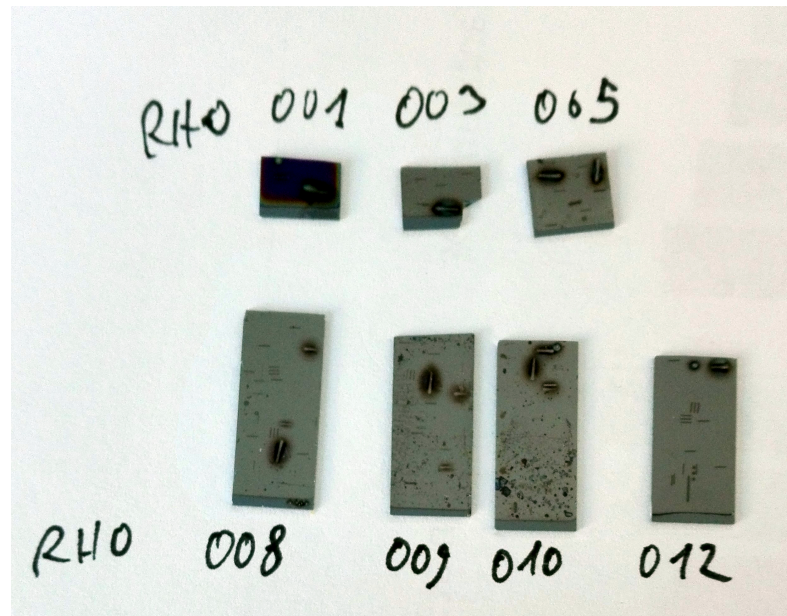


Figure 3.2: Image of the used samples.

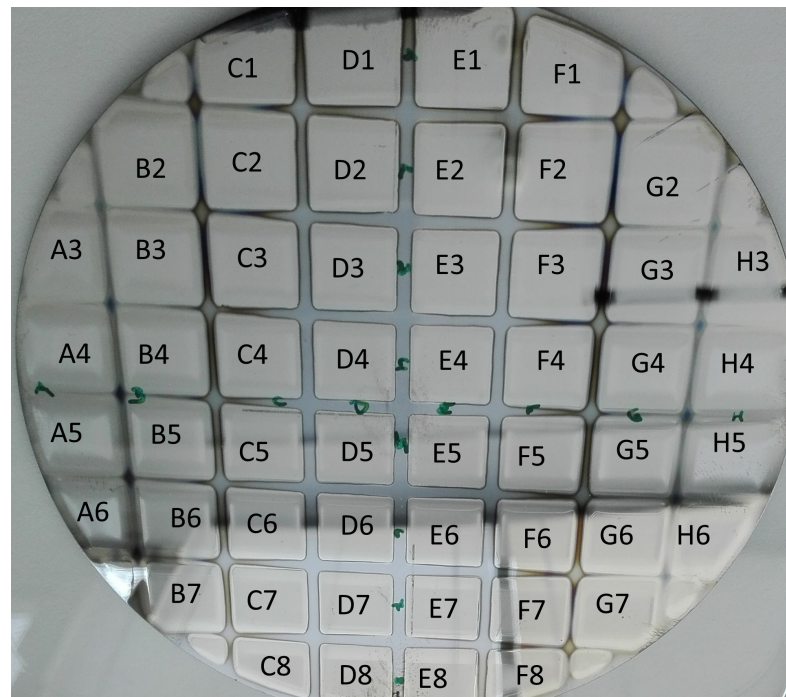


Figure 3.3: Image of the wafer with the fields of TaWB₂. The labels show the numbering of the fields used in the analysis.

3.3 Bulk measurements using liquid analysis

3.3.1 ICP-OES

ICP-OES measurements were carried out on an iCAP 6500 RAD (Thermo Fisher Scientific, USA). Samples were introduced with a ASX-520 autosampler (CETAC Technologies, USA) which was connected to the ICP with a Teflon tubing to a HF resistant sample introduction kit, consisting of a Miramist nebulizer (Thermo Fisher Scientific, USA), a PTFE spray chamber and a ceramic injector tube torch. For washing the tubing 3% HNO₃ and 0.3 % HF was used. For samples without HF, a high solid sample introduction kit was used. The plasma parameters are listed in Table 3.3. With ICP-OES background corrected intensities of the lines were recorded and quantified using external calibration with ICP single element standards, see Table 3.2, diluted with 3% HNO₃ 0.3 % HF.

Table 3.3: ICP-OES measurements parameters.

RF-Power	1350 W	
Radial observation height	10 mm	
Cool gas flow	12 L min ⁻¹	
Nebulizer gas flow	0.75 L min ⁻¹	
Auxiliary gas flow	0.4 L min ⁻¹	
Integration time visible	25 s	
Integration time UV (Al samples only)	10 s	
Replicates per sample	3	
Purge pump rate	1.6 mL min ⁻¹	
Analysis pump rate	0.8 mL min ⁻¹	
Measured lines	Quantifier line [nm]	Quality control line [nm]
Al	369.512	309.271
B	249.773	208.893
Ta	240.063	268.517
V	309.311	286.796
W	239.709	224.875

3.3.2 Sample digestion

The bulk analysis was carried out based on [10]. Silicon wafers were broken into pieces of about 2 mm side length, after scratching them with a diamond on the backside. Three replicates were prepared per sample. The pieces were put into 50 mL PP tubes and acid digested. Therefore, 1 mL nitric acid and 0.25 mL hydrofluoric acids were added and the samples were heated to 60 °C for about 10 min. The vessels were kept close to prevent loss from volatilization. After the digestion the samples were diluted with 20 mL of 3% HNO₃ 0.3 % HF and the PE tubes were directly loaded into the autosampler of the ICP-OES. Since elemental ratios were measured no internal standard was added.

3.4 Bulk measurements using direct solid sampling

3.4.1 LA-ICP-MS

In this study, a Thermo Scientific iCAP-Q (Thermo Fisher Scientific, USA), quadrupole ICP-MS equipped with a high linear range detector offering analog and digital counting mode [32] was used. The measurement parameters are given in Table 3.4.

Table 3.4: ICP-MS measurements parameters.

RF-Power	1400 W
Cool gas flow	12 L min ⁻¹
Nebulizer gas flow	0.8 L min ⁻¹
Auxiliary gas flow	0.4 L min ⁻¹
Dwell time	0.01 s
Measured Isotopes	¹⁰ B, ¹¹ B, ²⁷ Al, ²⁹ Si, ⁵⁰ V, ⁵¹ V, ¹⁸¹ Ta, ¹⁸⁰ W, ¹⁸² W, ¹⁸⁴ W

Table 3.5: Possible relevant interferences of the measured isotopes [33].

Isotope	Possible Interferences
¹⁰ B	-
¹¹ B	¹² C spread
²⁷ Al	¹² C ¹⁵ N ⁺ , ¹³ C ¹⁴ N ⁺ , ¹ H ¹² C ¹⁴ N ⁺ , ¹⁴ N ₂ spread
²⁹ Si	¹⁴ N ¹⁵ N ⁺ , ¹⁴ N ₂ ⁺ , ¹³ C ¹⁶ O ⁺ , ¹² C ¹⁷ O ⁺ , ¹² C ¹⁶ O ¹ H ⁺
⁵⁰ V	³⁴ S ¹⁶ O ⁺ , ³⁶ Ar ¹⁴ N ⁺ , ³⁵ Cl ¹⁵ N ⁺ , ³⁶ S ¹⁴ N ⁺ , ³² S ¹⁸ O ⁺ , ³³ S ¹⁷ O ⁺
⁵¹ V	³⁴ S ¹⁶ O ¹ H ⁺ , ³⁵ Cl ¹⁶ O ⁺ , ³⁸ Ar ¹³ C ⁺ , ³⁶ Ar ¹⁵ N ⁺ , ³⁶ Ar ¹⁴ N ¹ H ⁺ , ³⁷ Cl ¹⁴ N ⁺ , ³⁶ S ¹⁵ N ⁺ , ³³ S ¹⁸ O ⁺ , ³⁴ S ¹⁷ O ⁺
¹⁸¹ Ta	-
¹⁸⁰ W	¹⁸⁰ Ta
¹⁸² W	-
¹⁸⁴ W	-

The laser system used is a ESI NWR 213 (Electro Scientific Industries, Inc Portland, USA) with a flashlight pumped Nd:YAG laser. which is frequency quintupled to a wavelength of 213 nm. The ablations were carried out under Helium atmosphere with a gas flow of 650 mL min⁻¹. The ablation instrument is coupled to the ICP with a Teflon tube with an inner diameter of 2 mm. Argon nebulizer gas is mixed with the helium flow before entering the plasma. The fluence of the laser beam was noted as delivered by the instrument software. The laser was switched on an hour before the experiment was initialized, ensuring adequate warm up time. Samples were placed on an in-house build aluminum sample stage, loaded into the apparatus and flushed for 10 minutes with helium before starting the plasma of the ICP-MS. The plasma was warmed up for half an hour before starting the measurements. The ICP-MS settings were optimized on a daily basis maximizing the ¹¹⁵In signal of the NIST 612 CRM. Three microgrooves were measured for

each standard, 150 μm were chosen as spot size to completely ablate the groove. On the thin film samples (Figure 3.1 Figure 3.2) five laser lines we measured (Figure 3.4) with a small spot size (13 μm) to prevent the signals from getting too high, which could damage the detector and to have the absolute signals in the same range as for the microgroove standards. For the measurement of the whole wafer with varying composition Figure 3.3, three lines with parameters stated in Table 3.6 were on each field of the silicon wafer.

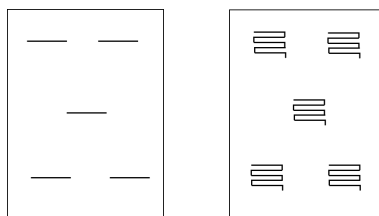


Figure 3.4: Scanning pattern for LA-ICP-MS measurements on the thin film samples. The meander pattern (right) was used to estimate homogeneity of the sample, the straight lines were used for the measurements .

Table 3.6: Laser ablation parameters.

	Microgroove preparation	Microgroove standard measurement	Thin film sample measurement
Fluence	1.3 J s^{-1}	3.0 J s^{-1}	17.6 J s^{-1}
Spot size	100 μm	150 μm	13 μm
He gas flow	150 mL min^{-1}		650 mL min^{-1}
Repetition Frequency		20 Hz	
Scanning speed	10 $\mu\text{m s}^{-1}$	100 $\mu\text{m s}^{-1}$	50 $\mu\text{m s}^{-1}$
Warm up time	3 s	15 s	15 s

3.4.2 LIBS

LIBS measurements were performed on a J200 Tandem (Applied Spectra, USA), equipped with a 266 nm nanosecond Nd:YAG laser and six Czerny-Turner CCD spectrometers, each 2048 pixel, covering a spectral range from 187 nm to 1047 nm. The system has a movable sample chamber with an integrated microscope, which allows to set the ablation patterns directly. Measurements can be carried out under air, helium or argon and the system is capable of being hyphenated to the ICP-MS to cover the advantages of both methods, the system was flushed with the inert gas for several minutes before the measurement to displace residual air. The laser is a Quantel Ultra (Quantel, USA), which is pulsed with a frequency up to 10 Hz and has a pulse energy of 24 mJ, which can be reduced by an attenuator. The spot can be focused to a diameter from 60 μm to 200 μm . Measurements of the microgroove standards and the thin film samples were carried out as line scans, where the scan speed, spot diameter and the repetition frequency determine the number

Table 3.7: LIBS measurements parameters.

Laser Energy	80 % = 19.2 mJ
Gate delay	0.5 μ s
Gate width	3 μ s
Stage speed	0.5 mm s ⁻¹
Spot size	100 μ m for microgrooves, 20 μ m for thin films with vanadium, 60 μ m for other thin films
Repetition Frequency	10 Hz
Measurement atmosphere	Argon
Gas Flow	1 L min ⁻¹
Main lines of Elements	Wavelengths [nm]
B	208.95, 249.67, 249.77 (these two lines could not be resolved)
W	232.831, 400.875, 407.43, 488.689, 429.46, 640.62
V	309.41, 356.61, 535.341, 609.020
Ta	240.063, 238.706, 268.51, 692.85
Al	307.46, 307.46, 394.40, 396.152
Si	243.515, 263.1282, 288.1579, 390.5523
Ar	763.5106, 772.3761, 738.3980
He	706.5190

of laser shots each point receives:

$$\text{shots per point} = \frac{\text{spotsize} * \text{repetition frequency}}{\text{stagespeed}} \quad (3.1)$$

The spectra of each laser shot were saved individually, typically of each sample 30 to 50 spectra were collected. The laser parameters are listed in Table 3.7. To quantify the LIBS data, the intensities of the peaks listed in Table 3.7 were integrated. A linear calibration was made by plotting the intensity ratios of the elemental lines versus the elemental ratios in the samples. Different combinations of elemental lines were evaluated to get the best calibration based on the R² value. The stoichiometry can be calculated from (3.2)

3.4.3 Surface profiles and SEM measurements

Profiles of the surfaces and ablation crater were obtained using an DektakXT stylus profilometer (Bruker, USA) with a tip of 2 μ m radius. Scanning electron microscopy was done using a FEI Quanta 200 (Thermo Fisher Scientific, USA) equipped with a Genesis (EDAX, USA) energy dispersive spectrometer.

3.4.4 Quantification strategy

The signals of the masses reported in Table 3.4 were recorded as a function of time during the scan of the groove or sample with the laser ablation apparatus. Two regions were set using the Qreg software, one in the time during the laser warm-up, without ablation as

a blank reference, and one during the ablation with a length of approximately 15 s. The mean counts per second in this region were calculated and ratios of the isotopes of interest plotted against the elemental ratios of the samples to get, a linear calibration. To calculate the relative elemental portions x , y and z from the elemental ratios $\frac{x}{y} = a$ and $\frac{y}{z} = b$ the following equations was used for the ternary samples:

$$x = \frac{ab}{ab + b + 1} \quad y = \frac{b}{ab + b + 1} \quad z = \frac{1}{ab + b + 1} \quad (3.2)$$

For the binary samples:

$$x = 1 - z \quad y = \frac{1}{1 + a} \quad (3.3)$$

3.4.5 Fabrication of microgrooves

Microgroove standards were prepared by laser ablation on the same apparatus used for the measurements. As substrates high purity silicon (100) wafers (Infineon, Austria), 1 cm × 1 cm and Makrolon® (Bayer AG, Germany) polycarbonate were used. Silicon wafers were broken into 0.5 cm × 1 cm pieces to utilize the space on the sample stage efficiently. Makrolon is delivered as plates of a thickness of 1 mm and were cut into pieces of 1 cm × 0.5 cm with a lever cutting machine.

After the shooting, the microgroove standards were placed in a water ultrasonic bath for 10 min to remove ablation debris. For the calibration the elemental ratios of standard solutions was used. For first experiments the Merck ICP-Standard solutions (see Section 3.1) were used. It was found necessary to increase the signal of the standards, so concentrated standard solutions were prepared. To overcome solubility problems, the starting materials and the composition of the solution have to be carefully chosen. For tungsten, a sodium tungstate solution in water was prepared with a concentration of about 0.42 mol/g, for boron a boric acid solution of 0.41 mol/g, for aluminum, an aluminum nitrate nonahydrate solution of 0.3 mol/g, for vanadium, vanadium(V)oxide was dissolved in a 10% sodium hydroxide solution to give a concentration of 0.34 mol/g. For the tantalum standard 0.1234 g tantalum powder were dissolved in 150 µL nitric acid and 200 µL hydrofluoric acid and diluted with 10 mL of water to give a solution of 0.06 mol/g. The concentration of the standard solutions were determined using ICP-OES after dilution by a factor of 500 and calibration by the certified ICP standards. The three element standards were prepared gravimetrically in 1 mL test tubes. The volume of the standard solution was chosen to be between 100 µL to 200 µL. To improve the solubility and to stabilize the solution to the Ta/W/B standards 200 µL of 2% HF, to the Al/W/B standards 100 µL of a 10% NaOH and to the V/W/B standards 100 µL of a 1% NaOH solution were added. The added sodium hydroxide for the VWB and AlWB systems maintains the pH in the alkaline range, where aluminum is stable as $[\text{Al}(\text{OH})_4]^-$ and the added tungsten and boric acid are present as anions. For the TaWB system tantalum was dissolved with hydrofluoric acid to stabilize it as fluoro complex in solution. The addition of further diluted HF prevents the precipitation when tungsten is added. Probably tungsten itself forms a fluoro complex and would pull away fluorine from tantalum. The standards were carefully homogenized and 20 µL were placed onto the microgrooves, excess liquid was removed with a rubber

spatula, so that sample only residues in the groove. After a short drying the samples were measured in the laser ablation apparatus.

4 Results and Discussion

4.1 Liquid analysis

The samples dissolved fast in the HNO_3/HF mixture. The composition of the samples is listed in the Appendix. The liquid OES measurements were treated as reference values during this thesis, the small standard deviation between the three replicates of the sample suggests that there is no large-scale trends or a random error in the method. However, it has to be kept in mind that neither a reference material, nor a standard method exists for the materials under investigation, so that systematic errors in the method could not be excluded. ICP-OES is an established method, so the main source of error lies in the dissolution process, where for example a volatilization of a compound remains possible.

4.2 Development of a calibration approach using microgrooves

4.2.1 Choice of material and preparation

The microgrooves were optimized to give a constant signal over their whole length. The parameters stated in Table 3.6 give a good compromise between speed of production and quality of the profiles. In Figure 4.1 the signals of tungsten and boron, as well as their ratio, are shown in a LA-ICP-MS measurement over the groove. It can be seen that the signals as well as the ratios of the signals are constant over the groove. The overshoot of the signal at the beginning of the ablation is an artifact stemming from the warm-up of the laser. Cross profiles of the microgrooves, measured by stylus profilometer and SEM images, are shown in Figure 4.2. The groove in Makrolon is much deeper and has a more regular appearance than the one in silicon. Further Makrolon does not show an accumulation of redeposited material on the edge of the groove. First experiments showed that the most important factor to match the ratios in calibration and the thin film materials is that the signal intensities have to be in a similar range. This was achieved using a small laser beam for the thin film materials and a high concentration of the standard solutions. These high concentrations could only be achieved by preparing concentrated solutions of the elements; which provided an improvement of the signal intensity of a factor between 10 and 50 in comparison with the stock ICP standard solutions. For the ternary systems the right parameters for the solutions had to be found to prevent precipitation. The high concentration of the standard solution poses no problem during the spreading in the microgrooves and yielded a smooth signal during ablation.

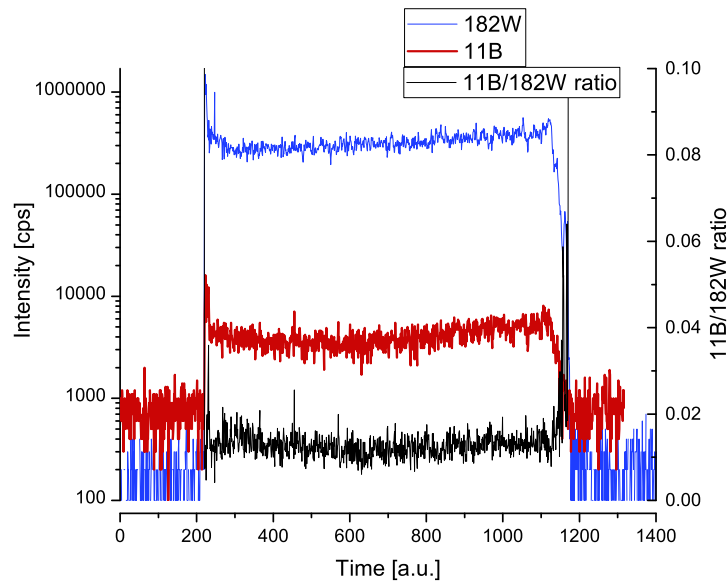


Figure 4.1: Example of the ICP-MS signal from the laser ablation scan over a microgroove.

4.2.2 Optimization of LA-ICP-MS analysis

The parameters of the laser ablation were different for the microgrooves and the thin film samples. Primarily experiments showed that to get reasonable results the differences of the absolute signals between the standards and the samples must be of the same order of magnitude. A small ($13\ \mu\text{m}$) laser spot diameter was chosen for the thin film measurements. Measurements of meander patterns (see Figure 3.4) showed that the signals are smooth and that no larger inhomogeneities on the small scale exist. Therefore five single lines Figure 3.4 were distributed evenly over the sample for further measurements. No clear trends in the signals over the wafers have been observed, although there exists some variation (see error bars in Figure 4.5). A laser high energy ($17.6\ \text{J}/\text{cm}^2$) was chosen to ablate a sufficient depth of the samples, compare Figure 4.4. Although on some samples a oxide film could be seen, no effect of this for the measurement could be observed. Therefore, the same patten was ablated two times and the second pass showed the same results as the first. Due to the rather high thicknesses of the samples ($> 1\ \mu\text{m}$) and the good mechanical properties of the films, it was not possible to shoot through the thin films and see a silicon signal with line scans. Spot scans revealed that about 15 to 20 laser shots per location would have been needed to fully penetrate the layers. The scan speed and the helium gas flow were optimized to get a reasonable smooth signal. In Figure 4.4 the depth profile of a ablation crater after two ablation passes can be seen. It has a depth of approx. $1.6\ \mu\text{m}$, so it can be estimated that for a single pass about $0.8\ \mu\text{m}$ are ablated, which is below the thickness of the films (compare Table A.1).

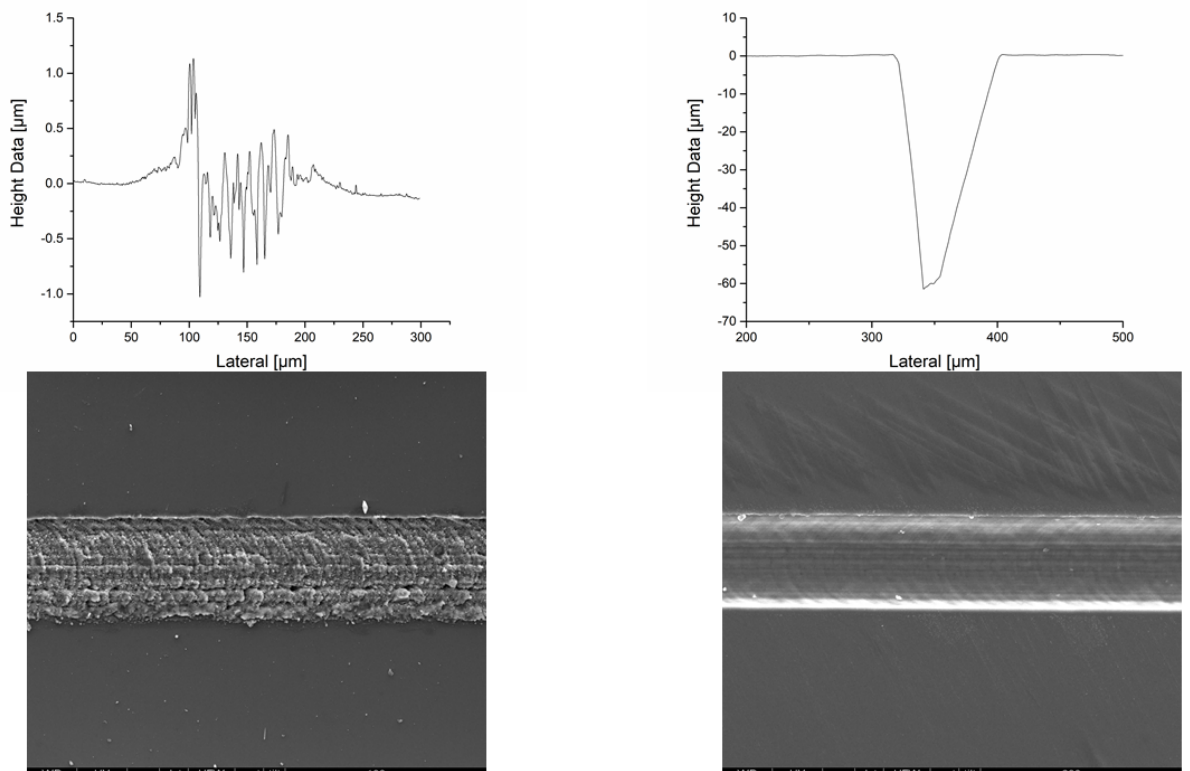


Figure 4.2: Upper row: profiles of the microgrooves in silicon (left) and Makrolon (right), lower row: SEM images of the microgrooves in silicon (left) and Makrolon (right).

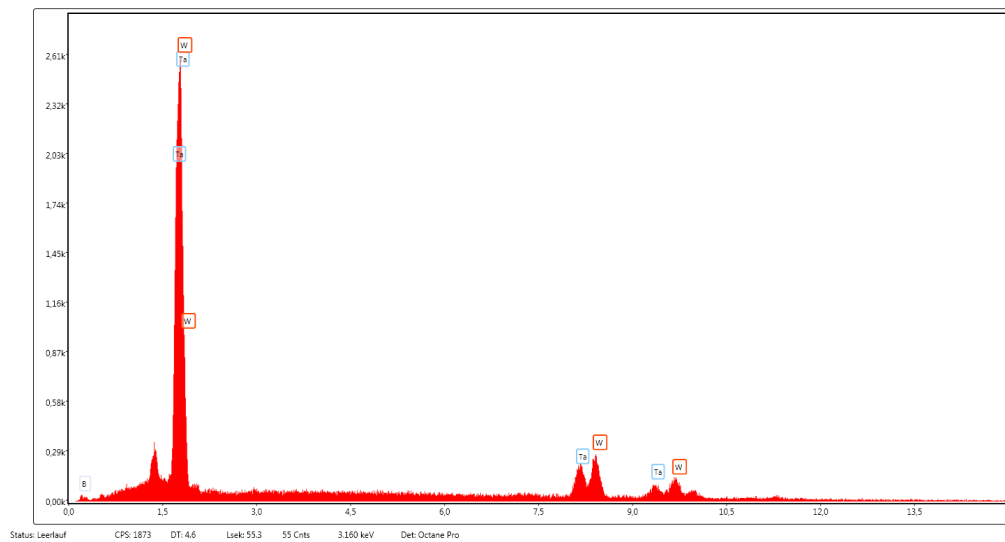


Figure 4.3: X-ray spectrum obtained by electron probe micro analysis (EPMA) of the FC11 TaWB₂ sample. Note that the boron peak is hardly visible and quantitative determination of the boron content are therefore not possible.

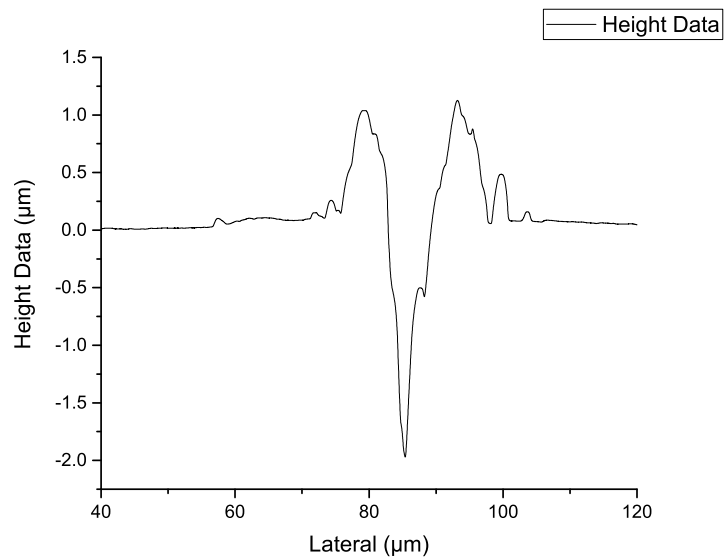


Figure 4.4: Depth profile of a laser ablation crater in the Rho008 sample after two passes of the laser. The parameters were 13 μm spot size, a scanning speed of 50 μm/s and a fluence of 17.6 J s⁻¹.

4.2.3 Microgroove calibration

It was possible to obtain a calibration with the elemental ratios for all investigated systems, see Figure A.1, Figure A.3, Figure A.2. The data points are the mean of the three grooves of one calibration standard. These calibrations were recorded with the Makrolon standards, which give a higher signal intensity due to their deeper profile (compare Figure 4.2). Further they are cheaper than the silicon wafers and can be cut easily in arbitrary sizes. Due to the thickness of the thin films, no silicon signal from the substrate could be observed during the line scan measurements, so that the proposed effect of the matrix matching with the substrate does not work. The direct comparison of the elemental ratios determined with OES with the LA-ICP-MS ratios generally showed a linear behavior. It has to be noted, that boron is a hard element to measure with ICP-MS due to its high ionization energy, which makes it prone to matrix effects, and its low mass which results in a low sensitivity. Deviations from the linear behavior, like for the V/B ratio in Figure A.6, exist. A general problem with the determination of the whole sample stoichiometry is the change of the material properties with changing composition. These properties include the thermal conductivity, tensile strength, ductility and the formation of oxide films, which all play a part during the laser ablation process. In Figure A.5 it can be seen that the samples with high aluminum content deviate from linear behavior, which is probably due to those effects. The oxide films on the surfaces proved to be of no importance for the measurement, a second ablation pass over yielded a comparable result as the first. The relative standard deviation of the elemental ratios between the ablated lines was below 10 % with no visible trend. This standard deviations did not have a considerable effect on the calculations of the concentrations, compare the error bars in Figure 4.7, Figure 4.5 and Figure 4.6 . In Figure A.5, Figure A.4 and Figure A.6 it is shown that it is possible in the current case obtain a good calibration when plotting the elemental ratios determined by liquid ICP-OES vs. the ICP-MS ratios, like it was used in [10]. The data points are the mean of the five lines on the thin film samples, see Figure 3.4. The measurement of the microgroove poses no problems. The signals are reasonable smooth and the relative standard deviation between the three grooves per standard is below 3 %. First experiments with the ternary standards suffered from the high number of outliers but this could be resolved by improving the formulation of the standards. It was found that the best way to determine the composition from the signals was to make use the elemental ratios for calibration and calculate the stoichiometry from those ratios with (3.2). Another approach tested was to make the calibration by normalizing each isotopic signal by the sum of the signals of all elements and plot it against the relative amount of that element in the standard, but this method did not result in linearity and was abundant. An attempt was made to build a PLS (Partial least square) by using the normalized Signals as predictors and the atomic fraction as response variable, but this also did not work well. The use of a multilinear model was hindered by the collinearity of the variables. It was considered to use a sputtered gold layer as a internal standard, but the use of elemental ratios made the normalization to a internal standard not possible.

4.3 Comparison of results

In the following part the obtained elemental fractions from liquid ICP-OES, LA-ICP-MS and ERDA are plotted side by side to compare the results. The error bars represent the standard deviation. The use of LA-ICP-MS with microgroove calibration generally gives reasonable results as seen in Figure 4.7, Figure 4.5 and Figure 4.6. For most cases the results are within a range of 5 % from the ICP-OES measurements. A general source of error for this case is the use of atomic percent as results, which couples the errors of the single measurements and leads to high relative errors for samples with a low amount of a certain element. In the following the results are discussed for each system.

4.3.1 AIWB, WB and AIB samples

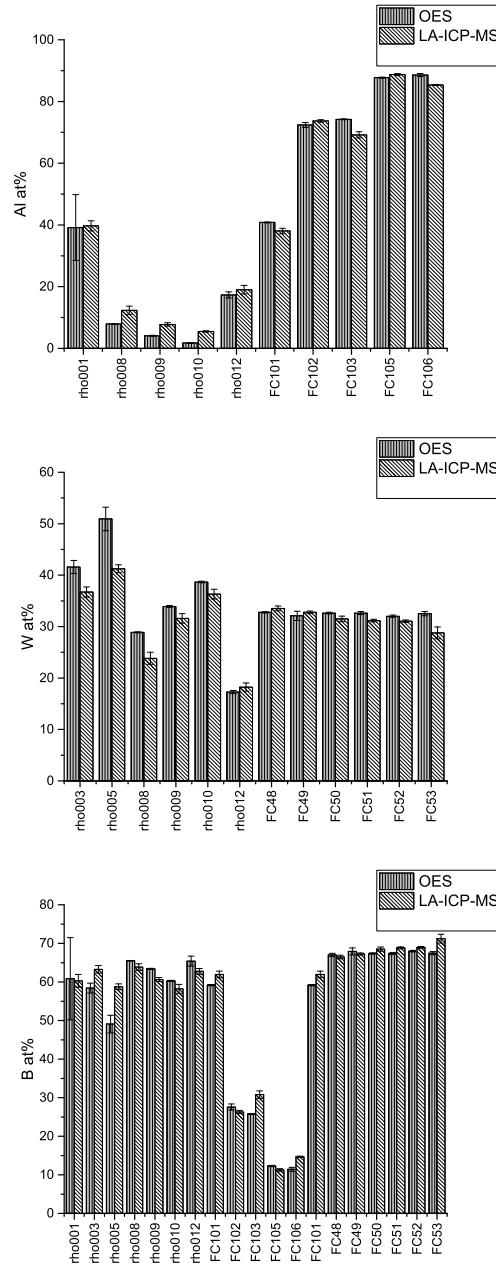


Figure 4.5: Comparison of the results for the AIWB, WB and AIB samples, error bars represent the standard deviation.

In Figure 4.5 it can be seen that the liquid ICP-OES and the microgroove LA-ICP-MS are in good agreement, especially for the boron results. The sample rho001 is the only one that shows a high standard deviation from liquid ICP-OES measurements. This sample

clearly shows an oxide layer (Figure 3.2 slight color gradient on the edge). The samples rho008, rho009 and rho010 have a rather low aluminum fraction. Due to the coupling of the errors for the elements this causes a rather large relative error.

4.3.2 VWB samples

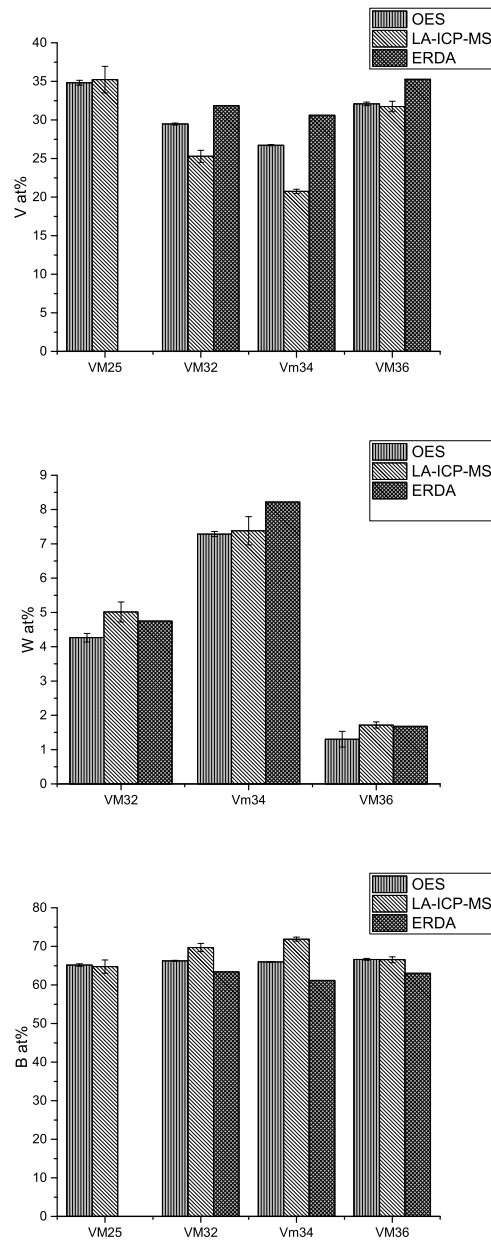


Figure 4.6: Comparison of the results for the VWB samples, error bars represent the standard deviation.

The VWB₂ samples Figure 4.6 show a good agreement between the OES, LA-ICP-MS and ERDA data. However certain trends can clearly be seen. LA-ICP-MS gives the lowest vanadium concentrations and the highest boron concentration. These systematic trends

may be explained by the different physical principles behind the methods, which lead to systematic errors.

4.3.3 TaWB samples

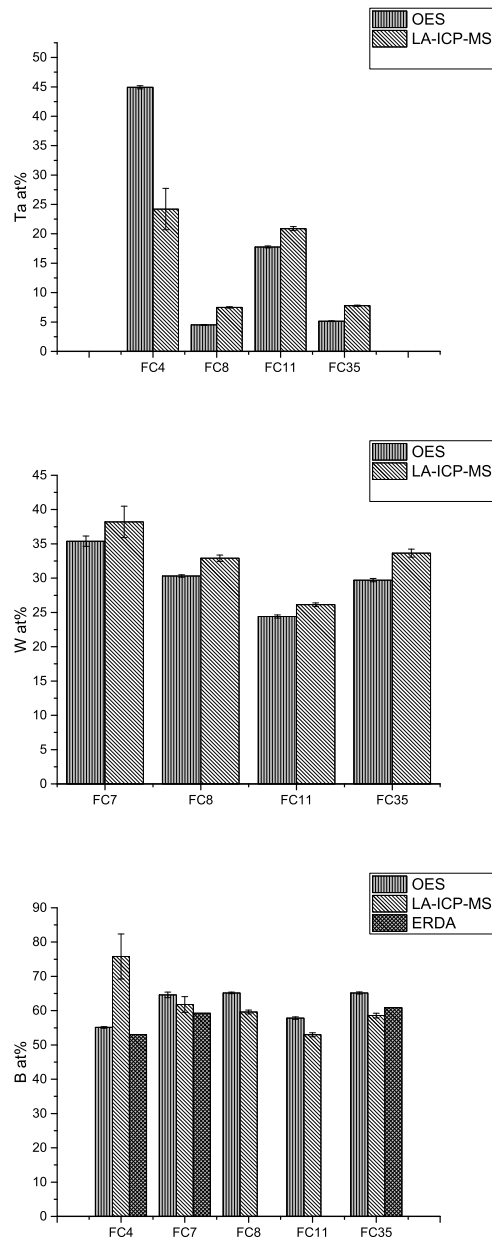


Figure 4.7: Comparison of the results for the TaWB samples, error bars represent the standard deviation, ERDA data are only reasonable for the boron content, see text for more details.

The TaWB₂ sample show a higher tungsten and tantalum content for the LA-ICP-MS measurements. The TaB₂ sample FC4 seems to be outliers, the OES measurements are in

agreement with the ERDA data, but differ from the LA-ICP-MS measurements. Because this sample has a very high standard deviation from the LA-ICP-MS results there may be because of some kind of inhomogeneity in the sample. The results for boron are in good accordance with the ERDA measurements, which is reported to have an absolute error of 1 at% [8]. The uncertainties for heavy elements are generally higher with ERDA [34], which further has a mass resolution incapable to distinguish tantalum and tungsten [8], which is a plausible explanation for the large deviations of the FC35 sample (OES: Ta 5.13 %, W: 29.70 %, B 65.15 %, ERDA: Ta: 36.373 % W: 2.737 % B: 60.89 %). For comparison a X-Ray spectrum of the sample FC11 is shown in Figure 4.3. it can be seen that a quantitative determination of boron is not possible due to the very low count rates.

4.4 Whole wafer measurements

Using the Makrolon calibration standards, the composition of each field of the wafer was determined. The numerical values can be found in Table A.5 in the Appendix. TaWB₂ samples digested and measured with ICP-OES were measured before the wafer to ensure the validity of the calibration and after to rule out instrumental drifts over the approximately 2.5 h measurement time. The compositions of each field are plotted in Figure 4.8 . A trend can clearly be seen.

4.5 LIBS

4.5.1 Optimization of parameters

LIBS measurements depend on several parameters as listed in Table 3.7. For the microgroove measurements a spot size of 100 μm was chosen to ablate the whole groove. The amount of sample in the microgroove is rather low and so the measurement conditions were optimized to give maximum signal to noise ratio for the lines of interest. This includes using argon atmosphere, which is known to yield higher intensities than helium atmosphere, [23] and the use of a intermediate long gate delay to keep the line intensities and the background in a balance. Using the same conditions to the thin films, the spot size has to be reduced, to prevent the detector from saturating. The device can focus the beam down to 60 μm , below a aperture is used to limit the beam to 20 μm , which also blocks the emitted light from reaching the detector. This yields in a large reduction of intensity. Despite the high energy of the laser, it was not possible to fully penetrate the thin film and to observe a silicon signal of the substrate. The silicon standards have the drawback that the silicon lines around 250 nm interfere with the boron lines at 249.77 nm, which make quantitative measurements hard (see Figure 4.9).

4.5.2 Calibration through line ratios

Because of the low signals it was only possible to obtain a reasonable calibration with the microgrooves with the VWB system on Makrolon, although using this calibration yielded no reasonable result for the thin films (Table 4.1). For all systems it was possible to obtain a linear relationship between the elemental ratios determined by ICP-OES and

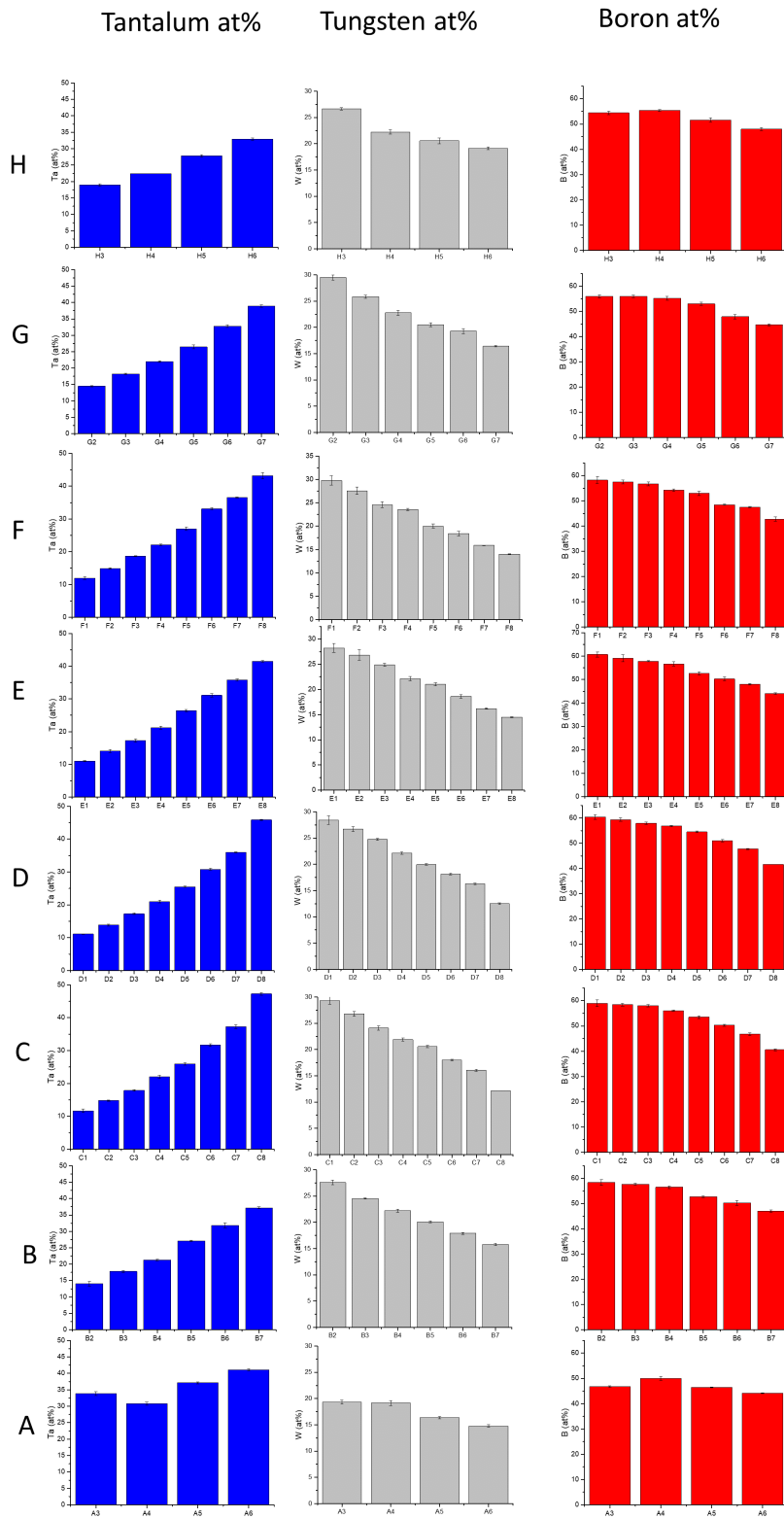


Figure 4.8: Composition of each field in the wafer with varying $Ta_{1-x}W_xB_2$ composition, see Figure 3.3 for a legend.

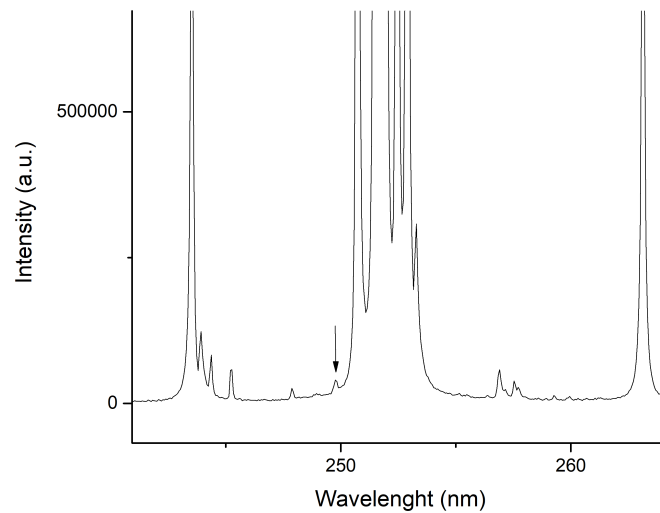


Figure 4.9: The boron line at 249.77 nm (arrow) overlaps with the base of the silicon peaks around 250 nm.

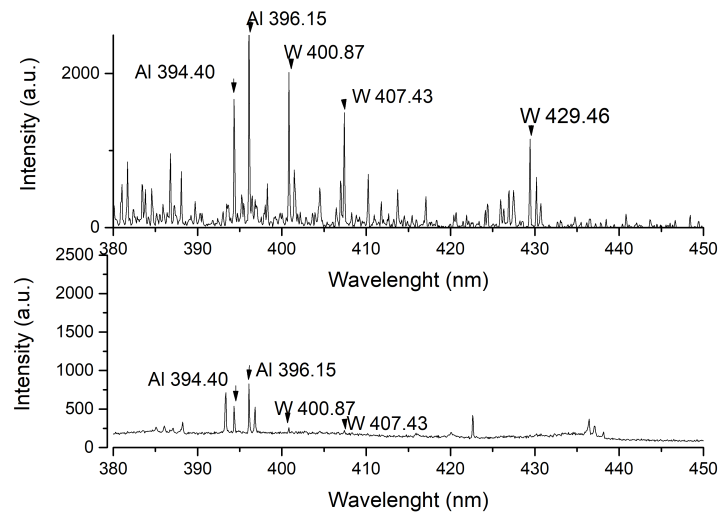


Figure 4.10: Comparison of a detail of the LIBS spectrum of a AlWB standard on Makrolon with the LIBS spectrum of the AlWB₂ sample Rho008, recorded with a spot size of 20 μm . It can be seen that the intensity of the tungsten lines in the Makrolon standard is very low compared with the thin film.

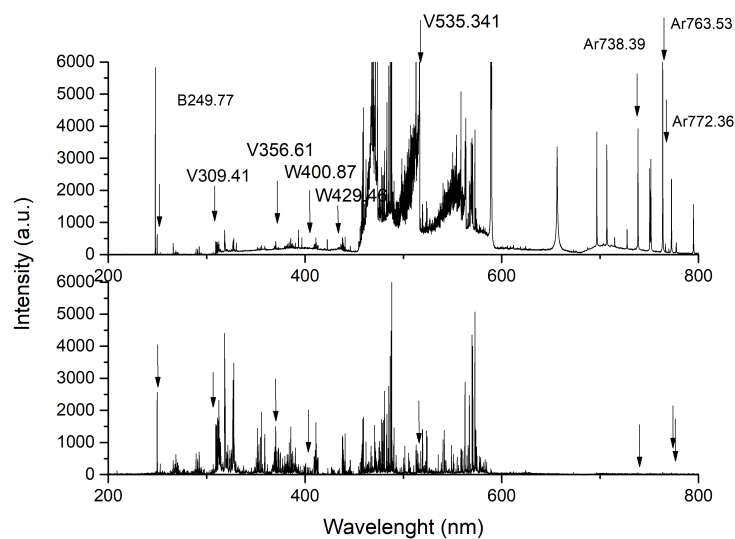


Figure 4.11: Comparison of the LIBS spectrum of a VWB standard on Makrolon with the LIBS spectrum of the VWB_2 sample VM32, which was recorded with a spot size of $20\ \mu\text{m}$, note that the intensity of the argon lines is greatly reduced due to the aperture in the beam path.

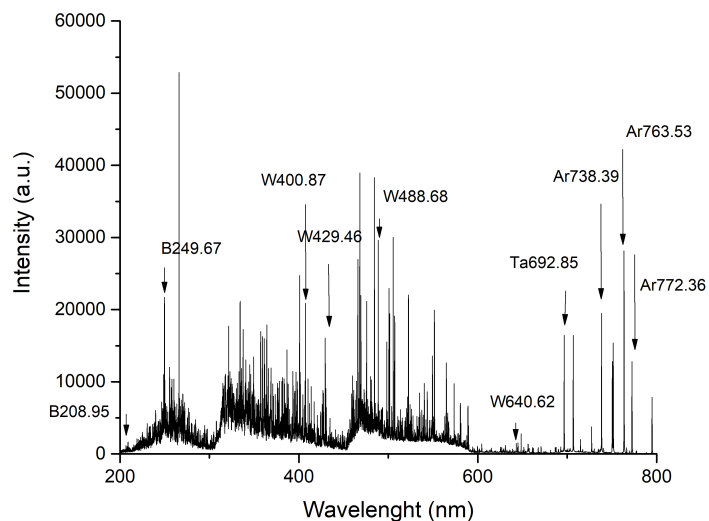


Figure 4.12: LIBS spectrum of the FC8 TaWB_2 sample recorded with a spot size of $60\ \mu\text{m}$.

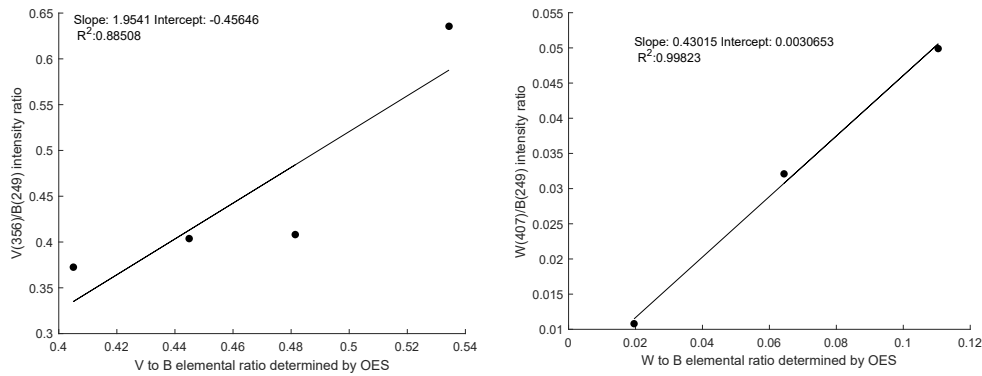


Figure 4.13: Calibration of VWB samples in LIBS system with OES.

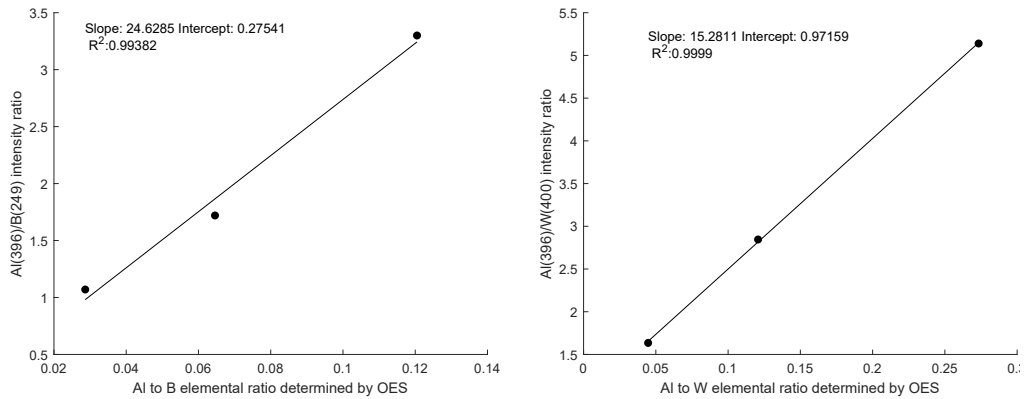


Figure 4.14: Calibration of AlWB samples in LIBS system with OES.

LIBS elemental line ratios. These are plotted in Figure 4.13, Figure 4.15 and Figure 4.14. Each point represents the mean signals from one measured line on the sample, obvious outliers were removed. Note that different elemental lines were chosen for each ratio. Vanadium and Tantalum show many elemental lines in the region between 300 and 500 nm, which overlap and seem to form a background. For tantalum the use of a line in another region (692.85 nm) reduces this limitation. For vanadium a small spot size had to be used (20 μm) to reduce the signal that only a low overlap occurs.

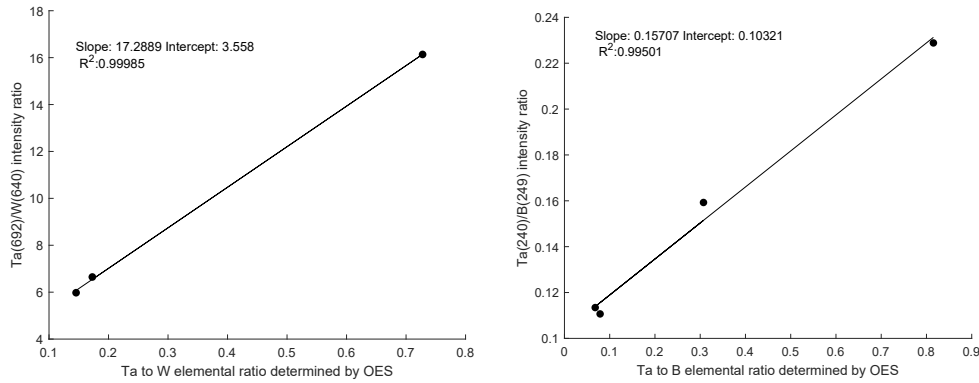


Figure 4.15: Calibration of TaWB samples in LIBS system with OES.

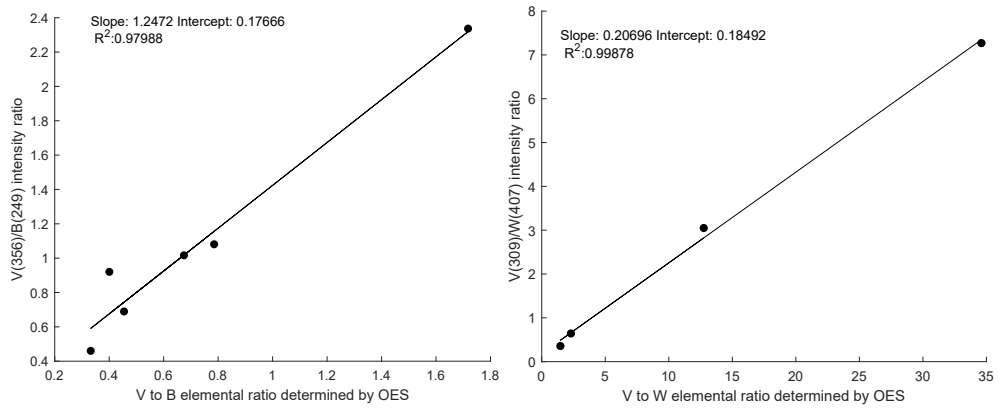


Figure 4.16: Calibration of VWB in LIBS system with microgrooves.

Table 4.1: Composition of the VWB₂ samples as determined by liquid ICP-OES and LIBS with the Makrolon standards.

	OES			LIBS		
	V	W	B	V	W	B
VM25	34.827	-	65.173	26.9	-	73.1
VM32	29.477	4.265	66.257	15.4	1	84.5
VM34	26.727	7.286	65.987	13.6	1	86.3
VM36	32.074	1.303	66.623	15.6	1	84.3

5 Conclusion and Outlook

Borides of the transition metals are promising class of materials. Their physical and chemical properties are influenced by their composition, especially the number of boron vacancies and the use of alloying metals. To understand these materials and to optimize the production process methods for determination of their composition are necessary. The measurement of boron is not possible with the often-used X-Ray based methods. Therefore more sophisticated methods are currently used, such as sample digestion with subsequent liquid analysis, which have the disadvantage that they are time consuming and require sophisticated, expensive instrumentation. The aim of this thesis was to find a method to makes these measurements easier and increases the sample throughput. Two approaches were explored: LA-ICP-MS and LIBS. The samples used in this thesis were tungstendiboride based ternary borides. As alloying elements aluminum, vanadium and tantalum were added. The sample were prepared by sputter coating the borides as thin films on silicon substrates.

LA-ICP-MS is a direct solid sampling method, which can measure the boride thin films without further sample preparation. To interfere from the signals to the composition of the samples matrix matched standards are necessary because LA-ICP-MS is a relative analytical method. The approach for calibration was to use microgrooves, small trenches in a surface filled with a standard solution. This approach combines the ease of using liquid standards, which can be simply prepared with the advantages of direct solid sampling, that no sample pretreatment is required. Primarily experiments showed that it is important that the absolute signals of the standards and the samples are of the same order of magnitude. This was achieved by using concentrated standard solutions, for which the composition had to be optimized to prevent precipitation. The microgrooves were prepared by laser micromachining. As substrates silicon wafers and Makrolon slides were used. Makrolon showed to be the material of choice. It exhibits a better ablation behavior, which yields in deeper grooves, which can hold more standard. The silicon microgroove would offer a better matrix matching with the samples, but this was of no relevance due to the high thickness of the samples. For all three systems, AlWB, VWB and TaWB, it was possible to obtain calibration functions based on the elemental ratios with a R^2 of about 0.99. The standards were used to determine the elemental ratios in the sample from which the overall stoichiometry was calculated. The results were in good agreement with the liquid ICP-OES measurements, which were performed as a reference method, the absolute deviations for the compositions was within 5 at% and a linear relationship between the ICP-MS and ICP-OES elemental ratios was observed. However, the validity of the liquid ICP-OES measurements was not confirmed and the data obtained must only be treated as a clue for the method comparison and not as certified values. For some of the film samples the composition was also determined using ERDA. A good agreement of the data with absolute deviations within 5 at% were found.

The LA-ICP-MS method with the microgroove calibration used in this thesis enables relatively fast measurements of a large number of samples with a comparable simple setup, compared with other methods used for the determination of boron (ERDA requires a large setup, liquid ICP-OES is rather laborious, other methods, like SIMS and XPS require much more elaborate quantification). With the solid sampling techniques spatial resolved measurements are possible, for example to investigate the homogeneity of the film. For the LIBS measurements, it was possible to obtain a linear relationship between the elemental ratios in the sample and the line ratios. The advantage of LIBS measurements is the comparable simple setup, which enables faster measurements and is cheaper than the LA-ICP-MS. A limitation of LIBS is the much higher limits of detection compared with LA-ICP-MS and the lower dynamic range. These are the reasons why the use of the microgroove standards is not feasible.

To improve the results of the LA-ICP-MS a better understanding of the ablation process and the plasma processes would be necessary to further improve the parameters. The optimization of the plasma parameters for boron was not evaluated, the standard settings optimized with Indium were used instead. A problem seems to be the high discrepancy between the sensitivity of boron and the other elements in ICP-MS. To resolve this issue laser ablation apparatus was coupled with the ICP-OES. The measurement of the thin film samples was working in principle, however due to the lower sensitivity of the OES detection it was not possible to use the microgroove standards. A large source of error stems from the coupling of the uncertainties for the overall composition. Especially when an element contributes only a minor fraction, the error from the elements with a higher proportion cause a large relative error for the minor element. To resolve this issue, probably more advanced mathematical methods are necessary. With the limited number of samples, the use of sophisticated mathematical methods was not feasible. For LIBS it is known that multivariate models, like PLS, give good results, but these require larger datasets to train and validate the model.

A Appendix

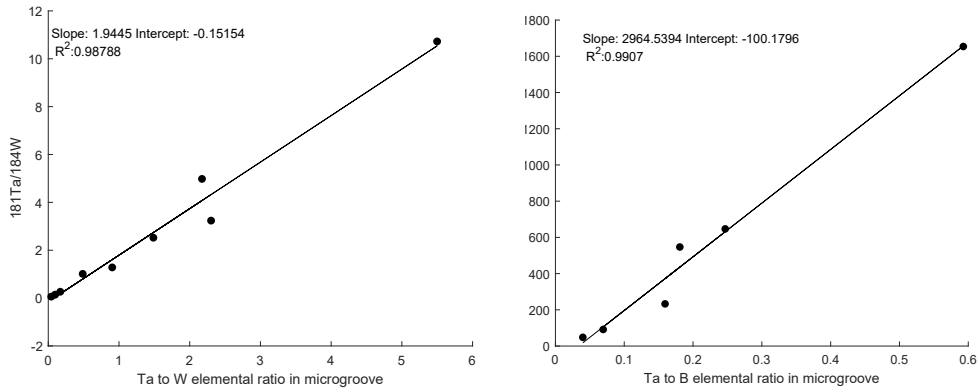


Figure A.1: Calibration of TaWB system with microgrooves.

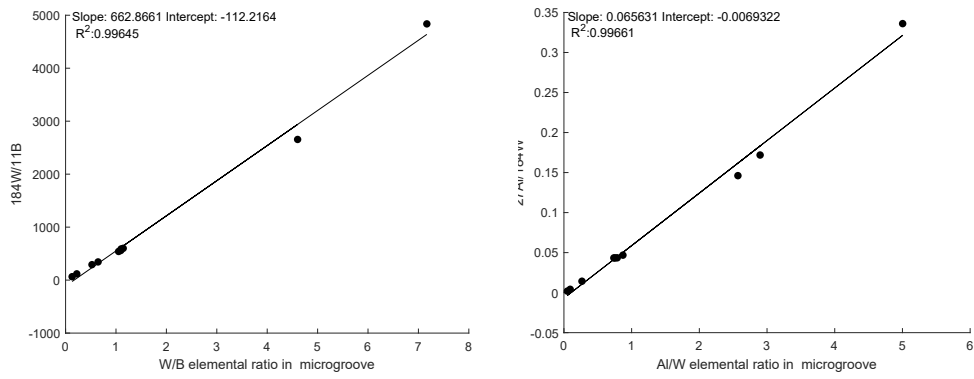


Figure A.2: Calibration of AlWB system with microgrooves.

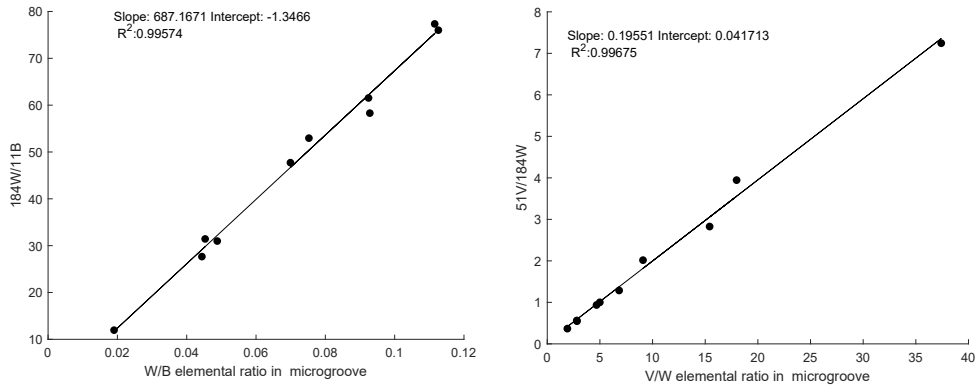


Figure A.3: Calibration of the VWB system with microgrooves.

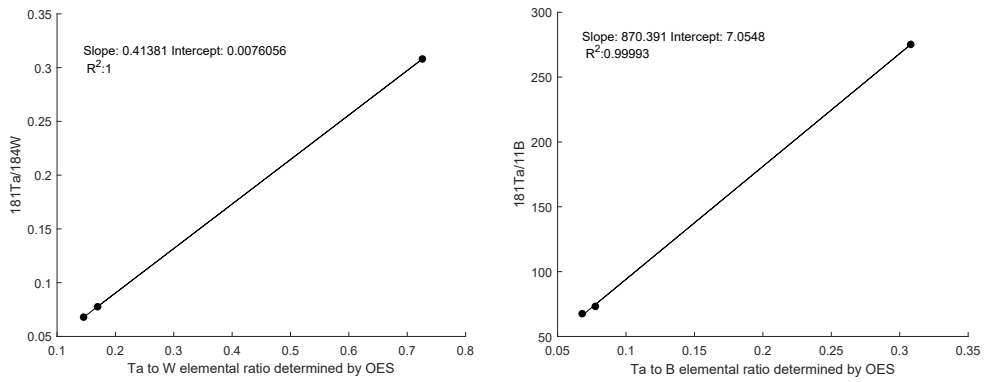


Figure A.4: Calibration of the TaWB system with OES.

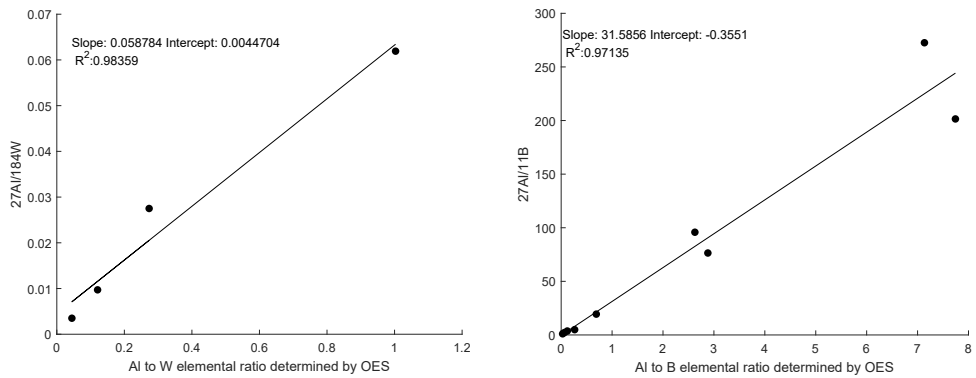


Figure A.5: Calibration of the AlWB system with OES.

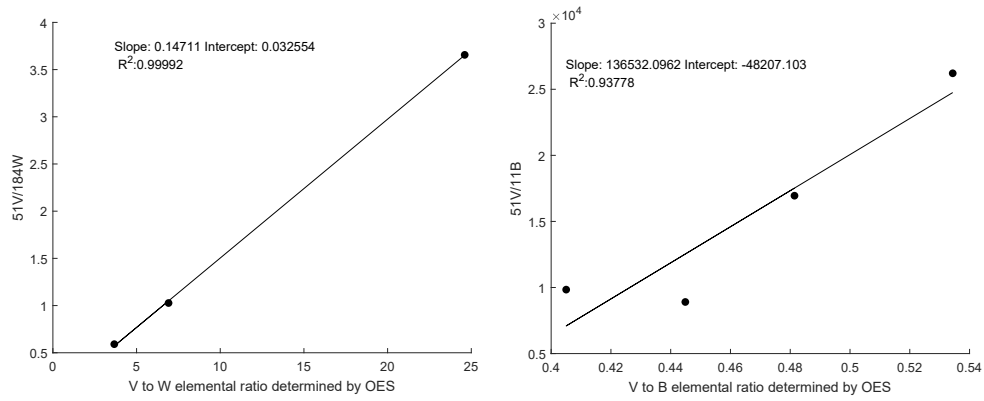


Figure A.6: Calibration of VWB system with OES.

Field	Ta at%	W at%	B at%
A3	33.84	19.34	46.81
A4	30.81	19.17	50.01
A5	37.13	16.37	46.48
A6	41.05	14.77	44.17
B2	14.03	27.59	58.37
B3	17.77	24.52	57.70
B4	21.25	22.23	56.50
B5	27.1	20.10	52.77
B6	31.81	17.90	50.28
B7	37.11	15.77	47.04
C1	11.67	29.33	58.98
C2	14.80	26.79	58.40
C3	17.88	24.11	58.00
C4	22.05	21.89	56.05
C5	25.97	20.54	53.47
C6	31.69	18.026	50.28
C7	37.23	16.04	46.72
C8	47.26	12.16	40.57
D1	11.118	28.43	60.45
D2	13.85	26.73	59.40
D3	17.276	24.78	57.94
D4	21.02	22.15	56.81
D5	25.523	19.96	54.50
D6	30.83	18.13	51.02
D7	35.97	16.28	47.73
D8	45.87	12.51	41.61
E1	11.04	28.21	60.73
E2	14.10	26.86	59.04
E3	17.32	24.87	57.80

E4	21.17	22.13	56.69
E5	26.40	21.02	52.57
E6	31.11	18.61	50.27
E7	35.78	16.19	48.02
E8	41.485	14.47	44.04
F1	11.95	29.77	58.26
F2	14.90	27.55	57.53
F3	18.68	24.58	56.73
F4	22.11	23.57	54.31
F5	26.972	20.026	53.00
F6	33.06	18.44	48.49
F7	36.52	15.89	47.57
F8	43.14	14.02	42.79
G2	14.49	29.49	56.01
G3	18.22	25.83	55.94
G4	22.00	22.78	55.21
G5	26.45	20.52	53.02
G6	32.80	19.29	47.90
G7	38.90	16.40	44.69
H3	18.95	26.64	54.40
H4	22.39	22.24	55.35
H5	27.81	20.56	51.61
H6	32.91	19.12	47.96

Table A.5: Composition of the fields of the $\text{Ta}_{1-x}\text{W}_x\text{B}_2$ wafer, the numbering of the fields can be seen in Figure 3.3.

Table A.1: Overview of the used XWB_2 samples, their approximate composition, film thickness and phase composition (s-> single phased, d-> double phased).

Name	Composition	Target current	Thickness [μm]	XRD Phase composition
FC4	TaB_2		2.9	d \rightarrow t-TaB + h-TaB ₂ (sg191)
FC8	$Ta_{0.8}W_{0.2}B_2$		3.4	d \rightarrow t-TaB + h-TaB ₂ (sg191)
FC11	$Ta_{0.5}W_{0.5}B_2$		3.7	d \rightarrow h-WB ₂ (sg191) + h-TaB ₂ (191)
FC35	$Ta_{0.2}W_{0.8}B_2$		4.1	s \rightarrow h-W-Ta-B ₂ (sg191)
FC7	WB_2		4.7	s \rightarrow h-W-Ta-B ₂ (sg191)
VM25	VB_2		1.6	s \rightarrow h-VB ₂ (sg191)
VM36	$V_{0.95}W_{0.05}B_2$		1.7	s \rightarrow h-VWB ₂ (sg191)
VM32	$V_{0.87}W_{0.13}B_2$		2.0	s \rightarrow h-VWB ₂ (sg191)
VM34	$V_{0.79}W_{0.21}B_2$		2.3	s \rightarrow h-VWB ₂ (sg191)
rho008	AlB_2/WB_2	150/75 mA	1.0	s \rightarrow h-AlWB ₂ (sg191)
rho003	WB_2		unknown	s \rightarrow h-WB ₂ (sg191) + t-WB ₂ (sg194)
rho005	WB_2		unknown	d \rightarrow h-AlWB + t
rho001	AlB_2/WB_2		unknown	unknown
rho009	AlB_2/WB_2	150/150 mA	1.7	s \rightarrow h-AlWB ₂ (sg191)
rho010	AlB_2/WB_2	75/150 mA	1.5	s \rightarrow h-AlWB ₂ (sg191)
rho012	AlB_2/WB_2	unknown	1.0	unknown

Table A.2: Composition of the TaWB₂ samples as determined by liquid ICP-OES, LA-ICP-MS with calibration through the microgrooves and the provided ERDA data, the values are in atomic percent.

	OES			LA-ICP-MS			ERDA		
	Ta	W	B	Ta	W	B	Ta	W	B
FC4	44.93	-	55.11	24.20	-	75.79	46.9	-	53.1
FC7	-	35.385	64.574	-	38.20	61.79	-	40.7	59.3
FC8	4.51	30.32	65.16	7.48	32.90	59.60	no data	no data	no data
FC11	17.766	24.41	57.823	20.88	26.13	52.98	no data	no data	no data
FC35	5.13	29.70	65.15	7.76	33.64	58.58	36.373	2.737	60.89

Table A.3: Composition of the AlWB, AlB and WB samples as determined by liquid ICP-OES, LA-ICP-MS with calibration through the microgrooves, the values are in atomic percent.

	OES			LA-ICP-MS		
	Al	W	B	Al	W	B
rho001	39.14		60.85	39.71	0	60.28
rho003		41.58	58.41	0	36.72	63.27
rho005		50.92	49.077	0	41.24	58.75
rho008	7.89	28.87	65.51	12.33	23.83	63.82
rho009	4.09	33.90	63.38	7.76	31.58	60.64
rho010	1.72	38.67	60.27	5.48	36.30	58.20
rho012	17.32	17.27	65.39	19.01	18.22	62.75
FC101	40.82		59.17	38.04		61.95
FC102	72.42		27.57	73.69		26.30
FC103	74.23		25.76	69.19		30.80
FC105	87.70		12.29	88.71		11.28
FC106	88.56		11.43	85.35		14.64
FC48		32.767	66.99		33.53	66.46
FC49		32.08	67.91		32.76	67.23
FC50		32.62	67.37		31.486	68.51
FC51		32.62	67.37		31.16	68.83
FC52		32.01	67.98		31.05	68.94
FC53		32.52	67.47		28.77	71.22

Table A.4: Composition of the VWB₂ samples as determined by liquid ICP-OES, LA-ICP-MS with calibration through the microgrooves and the provided ERDA data, the values are in atomic percent.

	OES			LA-ICP-MS			ERDA		
	V	W	B	V	W	B	V	W	B
VM25	34.827	-	65.173	35.23	-	64.77	-	-	-
VM32	29.477	4.265	66.257	25.28	5.015	69.70	31.86	4.75	63.39
VM34	26.727	7.286	65.987	20.74	7.381	71.87	30.6	8.22	61.18
VM36	32.074	1.303	66.623	31.74	1.717	66.54	35.27	1.68	63.04

B List of abbreviations

AC	Alternating current
AES	Auger Electron Spectroscopy
CCD	Charged coupled device
CID	Charge injection device
CRM	Certified reference material
CVD	Chemical vapor deposition
DC	Direct Current
EPMA	Electron probe micro analysis
ERDA	Elastic recoil detection analysis
HF	High frequency/ hydrofluoric acid
ICP-MS	Inductively coupled plasma mass spectrometry
ICP-OES	Inductively coupled plasma atomic emission spectroscopy
KED	Kinetic energy discrimination
LA-ICP-MS	Laser ablation inductively coupled plasma mass spectrometry
LIBS	Laser induced breakdown spectroscopy
Nd:YAG	Neodymium-doped yttrium aluminum garnet
ppb	Parts per billion
ppm	Parts per million
ppt	Parts per trillion
PTFE	Polytetrafluoroethylene
PVD	Physical vapor deposition
RF	Radio frequency
SIMS	Secondary ion mass spectrometry
TOF	Time of flight
XPS	X-Ray photoelectron spectroscopy
XRD	X-Ray Diffraction

Bibliography

- [1] C. Mitterer, "Borides in Thin Film Technology," *Journal of Solid State Chemistry*, vol. 133, no. 1, pp. 279–291, 1997.
- [2] H. Euchner, P. H. Mayrhofer, H. Riedl, F. F. Klimashin, A. Limbeck, P. Polcik, and S. Kolozsvari, "Solid solution hardening of vacancy stabilized $Ti_xW_{1-x}B_2$," *Acta Materialia*, vol. 101, pp. 55–61, 2015.
- [3] D. M. Mattox, "Chapter 7 - physical sputtering and sputter deposition (sputtering)," in *Handbook of Physical Vapor Deposition (PVD) Processing (Second Edition)*, D. M. Mattox, Ed., Second Edition, Boston: William Andrew Publishing, 2010, pp. 237–286.
- [4] A. J. Perry, "On the existence of point defects in physical vapor deposited films of TiN, ZrN, and HfN," *Journal of Vacuum Science & Technology A: Vacuum, Surfaces, and Films*, vol. 6, no. 3, pp. 2140–2148, 1988.
- [5] A. A. Goncharov, P. I. Ignatenko, V. V. Petukhov, V. A. Konovalov, G. K. Volkova, V. A. Stupak, and V. A. Glazunova, "Composition, Structure, and Properties of Tantalum Boride Nanostructured Films," *TECHNICAL PHYSICS*, vol. 51, no. 10, pp. 1340–1343, 2006.
- [6] A. I. Bazhin, A. A. Goncharov, A. D. Pogrebnyak, V. A. Stupak, and S. A. Goncharova, "Superhardness Effect in Transition Metal Diborides Films," *The Physics of Metals and Metallography*, vol. 117, no. 6, pp. 615–622, 2016.
- [7] C. Jiang, Z. Pei, Y. Liu, J. Xiao, J. Gong, and C. Sun, "Preparation and characterization of superhard AlB_2 -type WB_2 nanocomposite coatings," *Physica Status Solidi (a)*, vol. 210, no. 6, pp. 1221–1227, 2013.
- [8] V. Moraes, C. Fuger, V. Paneta, D. Primetzhofer, P. Polcik, H. Bolvardi, M. Arndt, H. Riedl, and P. H. Mayrhofer, "Substoichiometry and tantalum dependent thermal stability of α -structured W-Ta-B thin films," *Scripta Materialia*, vol. 155, pp. 5–10, 2018.
- [9] A. Limbeck, P. Galler, M. Bonta, G. Bauer, W. Nischkauer, and F. Vanhaecke, "Recent advances in quantitative LA-ICP-MS analysis: Challenges and solutions in the life sciences and environmental chemistry," *Analytical and Bioanalytical Chemistry*, vol. 407, no. 22, pp. 6593–6617, 2015.
- [10] A. Cakara, M. Bonta, H. Riedl, P. H. Mayrhofer, and A. Limbeck, "Development of a multi-variate calibration approach for quantitative analysis of oxidation resistant Mo-Si-B coatings using laser ablation inductively coupled plasma mass spectrometry," *Spectrochimica Acta - Part B Atomic Spectroscopy*, vol. 120, pp. 57–62, 2016, ISSN: 05848547. [Online]. Available: <http://dx.doi.org/10.1016/j.sab.2016.04.004>.

- [11] W. Nischkauer, F. Vanhaecke, and A. Limbeck, "Self-aliquoting micro-grooves in combination with laser ablation-ICP-mass spectrometry for the analysis of challenging liquids: quantification of lead in whole blood," *Analytical and Bioanalytical Chemistry*, vol. 408, no. 21, pp. 5671–5676, 2016.
- [12] H. Euchner and P. H. Mayrhofer, "Designing thin film materials-Ternary borides from first principles," *Thin Solid Films*, vol. 583, no. 1, pp. 46–49, 2015, ISSN: 00406090.
- [13] H. Duschanek and P. Rogl, "Critical assessment and thermodynamic calculation of the binary system boron-tungsten (B-W)," *Journal of Phase Equilibria*, vol. 16, no. 2, pp. 150–161, 1995.
- [14] W. Hayami, A. Momozawa, and S. Otani, "Effect of defects in the formation of AlB₂-Type WB₂ and MoB₂," *Inorganic Chemistry*, vol. 52, no. 13, pp. 7573–7577, 2013.
- [15] [Online]. Available: https://www.sigmaaldrich.com/content/dam/sigma-aldrich/product9/163/pvd_schematic_1.eps/_jcr_content/renditions/pvd_schematic_1-large.jpg (visited on 09/25/2018).
- [16] S. J. Hill, Ed., *Inductively Coupled Plasma Spectrometry and its Applications*. Blackwell Publishing Ltd, 2007.
- [17] Thermo Fisher Scientific Inc, *Thermo Scientific iCAP 7000 Plus Series ICP-OES: Innovative ICP-OES optical design*, 2017. [Online]. Available: <https://assets.thermofisher.com/TFS-Assets/CMD/Technical-Notes/tn-43333-icp-oes-optical-design-tn43333-en.pdf> (visited on 09/10/2018).
- [18] K. L. Linge and K. E. Jarvis, "Quadrupole ICP-MS: Introduction to instrumentation, measurement techniques and analytical capabilities," *Geostandards and Geoanalytical Research*, vol. 33, no. 4, pp. 445–467, 2009.
- [19] S. M. Nelms, *Inductively Coupled Plasma Mass Spectrometry Handbook*, S. Nelms, Ed. Blackwell Publishing Ltd, 2005.
- [20] J. W. Honour, "Benchtop mass spectrometry in clinical biochemistry," *Annals of Clinical Biochemistry*, vol. 40, no. 6, pp. 628–638, 2003.
- [21] R. E. Russo, X. Mao, J. J. Gonzalez, V. Zorba, and J. Yoo, "Laser ablation in analytical chemistry," *Talanta*, vol. 57, pp. 425–451, 2002.
- [22] L.-i. Plasmas, "Basics of the LIBS Plasma," in *Handbook of Laser-Induced Breakdown Spectroscopy*, D. A. C. Radziemski, r. J., and L., Eds., John Wiley & Sons, Ltd., 2006, ch. 2, pp. 23–52.
- [23] S. Musazzi and U. Perini, *Laser-Induced Breakdown Spectroscopy*. 2014, pp. 531–9.
- [24] J. Koch and D. Günther, "Review of the State-of-the-Art of Laser Ablation Inductively Coupled Plasma Mass Spectrometry," *Applied Spectroscopy*, vol. 65, no. 5, pp. 155–162, 2011.
- [25] W. D. Hahn and N. Omenetto, "Laser-Induced Breakdown Spectroscopy (LIBS), Part I: Review of Basic Diagnostics and Plasma - Particle Interactions," *Appl. Spectrosc.*, vol. 64, 335A–366A, 2010.

- [26] R. Wiens, S. Maurice, J. Lasue, O. Forni, R. Anderson, S. Clegg, S. Bender, D. Blaney, B. Barraclough, A. Cousin, L. Deflores, D. Delapp, M. Dyar, C. Fabre, O. Gasnault, N. Lanza, J. Mazoyer, N. Melikechi, P.-Y. Meslin, H. Newsom, A. Ollila, R. Perez, R. Tokar, and D. Vaniman, "Pre-flight calibration and initial data processing for the ChemCam laser-induced breakdown spectroscopy instrument on the Mars Science Laboratory rover," *Spectrochimica Acta Part B: Atomic Spectroscopy*, vol. 82, pp. 1–27, Apr. 2013.
- [27] A. J. Effenberger and J. R. Scott, "Effect of atmospheric conditions on LIBS spectra," *Sensors*, vol. 10, no. 5, pp. 4907–4925, 2010.
- [28] D. W. Hahn and N. Omenetto, "Laser-induced breakdown spectroscopy (LIBS), part II: Review of instrumental and methodological approaches to material analysis and applications to different fields," *Applied Spectroscopy*, vol. 66, no. 4, pp. 347–419, 2012.
- [29] T. Zhang, H. Tang, and H. Li, "Chemometrics in laser-induced breakdown spectroscopy," *Journal of Chemometrics*, no. July 2017, pp. 1–18, 2018.
- [30] J. Dong, L. Liang, J. Wei, H. Tang, T. Zhang, X. Yang, K. Wang, and H. Li, "A method for improving the accuracy of calibration-free laser-induced breakdown spectroscopy (CF-LIBS) using determined plasma temperature by genetic algorithm (GA)," *Journal of Analytical Atomic Spectrometry*, vol. 30, no. 6, pp. 1336–1344, 2015.
- [31] G. F. Bubert, Henning, and Surface, Eds., *Surface and Thin Film Analysis*, 2nd. Weinheim: Wiley-VCH Verlag & Co. KGaA, 2011.
- [32] Thermo Scientific, "Thermo Scientific iCAP RQ ICP-MS and high productivity for routine laboratories iCAP RQ ICP-MS The reliability , analytical performance and ease of use," Tech. Rep.
- [33] T. W. May and R. H. Wiedmeyer, "A Table of Polyatomic Interferences in ICP-MS," *Atomic Spectroscopy*, vol. 19, no. 5, pp. 150–155, 1998.
- [34] M. A. Arvizu, R. T. Wen, D. Primetzhofer, J. E. Klemberg-Sapieha, L. Martinu, G. A. Niklasson, and C. G. Granqvist, "Galvanostatic Ion Detrapping Rejuvenates Oxide Thin Films," *ACS Applied Materials and Interfaces*, vol. 7, no. 48, pp. 26 387–26 390, 2015.

List of Figures

2.1	Crystal structure of WB_2 in the 191 space group (left) and the 194 space group, from [12].	4
2.2	Phase diagram of the W-B system	4
2.3	Schematics of a simple sputter coating apparatus, from [15].	5
2.4	Schematics of the components of a ICP-OES system[17].	6
2.5	In ICP-OES the emitted light can be viewed radial to the torch (a), axial to the torch (C) or both axial and radial (b) [17].	7
2.6	Schematics of a simple Quadrupole ICP-MS, from [18].	7
2.7	Schematics of a quadrupole mass analyzer, from [20].	9
2.8	Schematics of a laser ablation apparatus, couples to a ICP-MS/OES, from [21].	11
2.9	Schematics of the microgroove concept	12
2.10	Schematics of a LIBS device, from [29].	14
3.1	Image of the used samples.	16
3.2	Image of the used samples.	17
3.3	Image of the wafer with the fields of $TaWB_2$. The labels show the numbering of the fields used in the analysis.	17
3.4	Scanning pattern for LA-ICP-MS measurements on the thin film samples	20
4.1	Example of the ICP-MS signal from the laser ablation scan over a microgroove.	25
4.2	Upper row: profiles of the microgrooves in silicon (left) and Makrolon (right), lower row: SEM images of the microgrooves in silicon (left) and Makrolon (right).	26
4.3	X-ray spectrum obtained by electron probe micro analysis (EPMA) of the FC11 $TaWB_2$ sample	27
4.4	Depth profile of a laser ablation crater in the Rho008 sample after two passes of the laser.	27
4.5	Comparison of the results for the AlWB, WB and AlB samples	30
4.6	Comparison of the results for the VWB samples	32
4.7	Comparison of the results for the TaVWB samples	34
4.8	Composition of each field in the wafer with varying $Ta_{1-x}W_xB_2$ composition	36
4.9	The boron line at 249.77 nm (arrow) overlaps with the base of the silicon peaks around 250 nm.	37
4.10	Comparison of a detail of the LIBS spectrum of a AlWB standard on Makrolon with the LIBS spectrum of the AlWB ₂ sample Rho008	37
4.11	Comparison of the LIBS spectrum of a VWB standard on Makrolon with the LIBS spectrum of the VWB ₂ sample VM32	38

4.12	LIBS spectrum of the FC8 TaWB ₂ sample recorded with a spot size of 60 μm.	38
4.13	Calibration of VWB samples in LIBS system with OES.	39
4.14	Calibration of AlWB samples in LIBS system with OES.	39
4.15	Calibration of TaWB samples in LIBS system with OES.	40
4.16	Calibration of VWB in LIBS system with microgrooves.	40
A.1	Calibration of TaWB system with microgrooves.	43
A.2	Calibration of AlWB system with microgrooves.	43
A.3	Calibration of the VWB system with microgrooves.	44
A.4	Calibration of the TaWB system with OES.	44
A.5	Calibration of the AlWB system with OES.	44
A.6	Calibration of VWB system with OES.	45

List of Tables

3.1	List of used chemicals.	15
3.2	List of used ICP Standard solutions from Merck	16
3.3	ICP-OES measurements parameters.	18
3.4	ICP-MS measurements parameters.	19
3.5	Possible relevant interferences of the measured isotopes [33].	19
3.6	Laser ablation parameters.	20
3.7	LIBS measurements parameters.	21
4.1	VWB ₂ samples with LIBS and microgrooves	40
A.5	Composition of the fields of the Ta _{1-x} W _x B ₂ wafer	46
A.1	Overview of the used XWB ₂ samples	47
A.2	Composition of the TaWB ₂ samples	48
A.3	Composition of the AlWB, AlB and WB samples	49
A.4	Composition of the VWB ₂ samples	50